LIQUID ANNULAR SEAL CFD ANALYSIS FOR ROTORDYNAMIC FORCE PREDICTION

ABSTRACT

Jeff Moore and Alan Palazzolo
Texas A & M
College Station, Texas

A commercially available code developed by CFD Research Corporation (CFDRC) in Huntsville under contract by the Marshall Space Flight Center is utilized to analyze a plain and grooved liquid annular seal. These type seals are commonly used in modern turbopumps and have a pronounced effect on the rotordynamic behavior of these systems. Accurate prediction of both leakage and dynamic reaction forces is vital to ensure good performance and sound mechanical operation.

The code SCISEAL developed by CFDRC is a generic 3-D, finite volume based CFD code solving the 3-D Reynolds averaged Navier Stokes equations. The code allows body-fitted, multi-block structured grids, turbulence modeling, rotating coordinate frames, as well as integration of dynamic pressure and shear forces on the rotating journal. The code may be used with the commercially available pre and post-processing codes from CFDRC as well.

To benchmark the code, comparisons are made with recent tests by Marquette (1995) for both a plain annular and multi-grooved liquid seals. Both leakage and dynamic force coefficients (stiffness, damping, and inertia) are measured at speeds up to 24,000 rpm and pressures drops approaching 7 MPa (1000 psid) using water as the test media. The CFD results are presented along with analytical predictions using bulk-flow fluid assumptions. The results show little improvement over bulk flow with CFD for the plain annular seal but with substantially increased computational effort for CFD. On the other hand, CFD better captures the recirculating nature of the grooved seal flow field resulting in much improved prediction compared to bulk flow.

References:

Marquette, O.R., 1995, "Experimental vs. Theoretical Comparison of the Static and Dynamic Characteristics of One Smooth and Two Grooved Liquid Annular Seals with L/D of 0.457." *Turbomachinery Laboratories, Mechanical Engineering Dept., Texas A & M University, TL-SEAL-5-95.*

Presentation Overview

Introduction

Annular seals have a pronounced effect on the rotordynamic response and stability of modern high performance turbomachinery. Accurate prediction of their dynamic forces and leakage is fundamental in producing robust machinery designs with minimal risk to vibration problems operating with maximum efficiency. Using modern computational fluid dynamic (CFD) techniques, the true flow field may be captured with a minimal amount of empirical input. Labyrinth or grooved seals are especially challenging due to the complex geometry, large pressure and velocity gradients, high turbulence intensity, and large recirculations present in the flow field all of which is inherently unsteady. By generating an eccentric three-dimensional, body fitted mesh of the geometry, a psuedo-steady solution may be obtained in the rotating reference frame that is attached to the whirling rotor. The net reaction force is calculated due to the given eccentricity (definition of impedance) for different ratios of rotor speed to whirl speed (whirl frequency ratio, WFR). These impedance forces contain a component normal and transverse to the rotor displacement, obtained by integration of the static pressure and shear stress distribution around the rotor, and are curve-fitted to a linear, second order model to yield the seal's stiffness, damping, and mass force coefficients (K_{xx}, K_{xy}, C_{xx}, C_{xy}, M_{xx}, M_{xy}).

CFD Code Description

The CFD code, SCISEAL, is utilized in this study and was developed by CFD Research Corporation under a grant from NASA Lewis Research Center. The code solves the 3D Reynolds averaged Navier-Stokes equations (see equations below) for both rotating and stationary frames of reference, using cylindrical, body fitted, structured grids of multi-domains. Both compressible and incompressible flow fields may be modeled using the latest turbulence models (standard k-ε, low Reynolds no. k-ε, Baldwin-Lomax, and two-layer k-ε). Law of the wall formulations model the sharp velocity gradients near the wall and are used with all turbulence models with the exception of the low Reynolds number model. The two-layer model is employed in this study, which models the turbulence diffusion near the wall (inner layer) using an algebraic expression, while the turbulence kinetic energy equation is applied in both the inner and outer layers. This model relaxes the requirement of maintaining the first node from the wall outside the laminar sublayer (ie. $y^+>11.5$), allowing more nodes to be placed in the tight seal land sections.

The code's generality allows modeling of all variety of seals types including plain annular, labyrinth, grooved, stepped, and even geometries of varying radius (ie. impeller shrouds, etc.). Assuming concentric, circular whirling, the impedance forces for varying whirl frequency ratios are calculated, as described above, yielding the rotordynamic force coefficients.

Literature Review

Traditional modeling techniques for annular seals utilize bulk-flow assumptions (see Black, 1969, and Childs, 1983). These models assume uniform velocity distributions for the steady analysis. Harmonic variations of the flow parameters are assumed around the circumference for the dynamic analysis and removes the circumferential (theta) dependence. Turbulence is handled using empirical wall shear stresses obtained from pipe flow studies including Hirs and Moody friction factor relationships, which are a function of the local Reynolds number. These methods are quite efficient, requiring only seconds of CPU time, and are accurate for plain annular seals. Modeling seals with separation and recirculations will usual result in poor predictions, however. Modification of the bulk-flow models for grooved seals has been done using multiple control volumes using a single vortex in the cavity with empirical shear stress

boundary conditions at the interface (Florjancic, 1990). Again, these techniques are efficient and accurate if "tuned" for a specific set of operating conditions using empirical data. As the operating conditions and geometry differ, typically so does the resulting predictions.

More recent techniques have utilized the rapidly maturing computational fluid dynamic analysis for modeling annular seals including Dietzen and Nordman (1986) Rhode, Hensel, and Guidry (1992), and Arghir and Frene (1997). All of these authors employ a coordinate transformation relation transforming the 3D equations of the eccentric rotor into 2D axisymmetric expressions. These techniques require a zeroth order solution and first order calculations at the different whirl frequency ratios. The procedure is efficient but the coordinate transformation is only valid for constant radius seal geometries, and the analysis ignore the variation of turbulence quantities around the circumference. Furthermore, only axisymmetric seal geometries may be modeled, preventing the modeling of swirl brakes for example. The 3D whirling method used in SCISEAL, developed by Athavale, et al. (1994), is more computationally intensive but is more general in the class of problems that may be solved.

Test Rig and Grooved Seal Description

This study focuses on a high pressure, seven-grooved liquid annular seal, which was tested by Marquette (1995) in the High Speed Seal Test Rig at Texas A & M University (see Figures 1 and 2). This seal was tested to speeds up to 24,600 rpm and pressures drops over 6 MPa (900 psid) and contains a shaft radius of 38.15 mm (1.5 in), clearance of 0.11 mm (4.3 mils), and an L/D of 0.457. The equally spaced grooves have dimensions 1.587 mm deep by 3.175 mm wide.

Results of CFD Analysis of Grooved Liquid Seal

The first approach taken was to model seal geometry and use "typical" boundary conditions at the inlet for the pressure loss factor (Ploss=0.1) and the inlet swirl ratio (ratio of fluid swirl to rotor surface speed, Wrat=0.45). Results are presented for four different grid densities, striving for a grid independent solution, and are summarized in Table 1. The Coarse Grid-1 refines the circumferential grid density, the Medium Grid refines the grid density in the seal groove, the Fine Grid-1 refines the grid in the seal land (tight clearance sections), and finally the Fine Grid-2 refines both the land and the groove. The medium grid requires about 1 minute per iteration on a SGI Indigo 2 (with R10000 64 bit MIPS processor, 195 MHz), while the Fine Grid-2 requires 2.2 minutes per iteration. Since SCISEAL utilizes an iterative solver; the time per iteration is proportional to the total node number. However, convergence rates are higher for the smaller models (less iterations required). The memory requirement is roughly the number of nodes in kilobytes (eg. Medium Grid requires about 100 megabytes of memory).

The velocity vectors in the seal cavity show a large, single vortex (Fig. 5) predicted using the medium grid. A close-up of the flow field entering the seal land is given in Fig. 6. Figure 7 shows a uniform static pressure drop through the seal. The transport equations for the turbulence kinetic energy (k) and the turbulence dissipation are solved simultaneously with the Navier-Stokes equations predicting large generation and dissipation of turbulence in the jet shear layer exiting the seal land and near the seal land entrance (Figs. 8-9). Accurate calculation of the Reynolds stresses at this jet/vortex interface is necessary to accurately predict the mean velocity profiles. The isotropic assumption of turbulence, assumed by the k-ε model, is well known not to exist in shear layers and is one of the sources of errors of the CFD calculation.

The circumferential variation of pressure displayed using an exaggerated mesh shows the effect whirl frequency ratio in Figures 10 and 11. Figure 10 shows a harmonic distribution of pressure fluctuating

from low to high while proceeding clockwise from the top. This statically eccentric seal (WFR=0.0) show similar characteristics as a plain journal bearing and creates a pressure field that both opposes displacement and pushes the rotor in the direction of whirl, creating positive direct and cross-coupled stiffness coefficients (K_{xx} and K_{xy}). This cross-section was taken in the first seal groove and changes somewhat through the length of the seal. At higher whirl frequency ratios (WFR=1.5), a nearly opposite pressure field emerges creating forces in the direction of displacement and whirl. This effect will become clear in the impedance force plots. Although ignored by some seal analysis techniques, the turbulent quantities do vary circumferentially for a whirling seal as shown in Figure 12.

At the entrance of the seal, a total pressure boundary condition is assumed allowing the axial velocity to naturally develop around the circumference as shown in Figure 13. This boundary condition captures the Lamakin effect, which is a source of positive stiffness. To capture the sudden loss of pressure due to the abrupt change in cross-section entering the seal, an inlet loss factor is assumed. The pressure drop is calculated by:

$$\Delta P = \frac{\rho}{2}\bar{U}^2(\zeta + 1)$$

Typical values of ζ range from 0.1 and as high as 0.7 (Athavale, et al., 1994).

As previously mentioned, care must be taken when choosing the node distribution to maintain the first node a proper distance away from the wall. This distance is a function of the flow field, necessitating a post-check of the non-dimensional y^+ values. Figures 14 and 15 show the y^+ values on both the rotor and cavity walls to be well within the range of the law of the wall.

Figures 16 and 17 compare the convergence rates of two different mesh densities, the Coarse Grid-1 and the Medium Grid, respectively. The coarse grid, which is half the size of the medium grid, demonstrates twice the convergence rate. Since the time per iteration is proportional to the number of nodes, the total time to convergence for the coarse grid is about 25% of the medium grid's CPU time.

Force Coefficients of Analysis I

Table 2 compares the SCISEAL computation (using medium grid) of force coefficients and leakage with both experimental results as well as the 3-control volume (3-CV) prediction of Marquette (1995) for a speed of 10,200 rpm and a pressure drop of 4.14 MPa (600 psid). The experiment measures essentially no direct stiffness with a positive cross-coupled stiffness. The CFD analysis gives reasonable prediction and much improved stiffness prediction over the 3-CV results. Direct and cross-coupled damping, however, is under-predicted by the CFD analysis as is the inertia. The whirl frequency ratio (at neutral stability), which is a measure of the stability of the seal, shows good prediction between CFD and experiment.. The CFD under predicts the leakage rate by about 10%. The impedance forces from six whirl frequency ratios (0.0, 0.25, 0.5, 0.75, 1.0, and 1.5) are used to calculate the force coefficients by curve-fitting the results to a second order polynomial using the following expressions:

$$\bar{F}_n = \frac{F_n}{\epsilon} = -K - c\omega + M\omega^2$$

$$\bar{F}_t = \frac{F_t}{\epsilon} = k - C\omega - m\omega^2$$

where, ϵ = eccentricity
K, C, M = direct stiffness, damping, mass
k, c, m = cross-coupled stiffness, damping, mass

The plot of impedance versus whirl speed shows a nice curve fit by the second order functions.

To evaluate the effect of rotor speed and pressure, the force coefficients are evaluated at 24,600 rpm and 6.20 MPa (900 psi) shown in Table 3. The direct stiffness is under predicted somewhat, but the CFD results show significantly improved prediction of cross-coupled stiffness compared to the 3-CV results. Again, the damping is under predicted resulting in an over-prediction of whirl frequency ratio at neutral stability. The over prediction of 60% is still a large improvement over the 1100% error of the 3-CV. The leakage is again under-predicted by about 11%, similar to the 3-CV. The 3-CV analysis contains many "knobs" which may be adjusted (ie. jet divergence angle and shear stress parameters) to yield reasonable prediction. Marquette (1995) used a negative jet divergence angle, selected by leakage comparison, indicating the vortex deflects the jet. The opposite is predicted by CFD as shown in Figure 6.

A mesh density study is performed to verify if the preceding results are grid independent solutions. Table 4 compares the stiffness and leakage predictions for the five different mesh densities (see Table 1 for definition of each). The cross-coupled stiffness shows strong sensitivity to the number of nodes used across the seal land comparing the Medium and Fine Grid-1, then changes little with further refinement. This study shows that a mesh density at least equal to the Fine Grid-1 is required for reasonable cross-coupled stiffness prediction and now over-predicts the experimental value. Good leakage prediction is accomplished with even the coarsest grid. Table 5 shows the damping and inertial coefficients to be less sensitive to mesh density (only values up to the medium grid are computed).

Force Coefficients of Analysis II

Since the prediction of cross-coupled stiffness is a strong function of the inlet swirl ratio (Wrat), an upstream, axisymmetric (2D) calculation is performed in order to better quantify the flow conditions entering the seal. The upstream geometry was obtained and coupled to the 2-D model of the grooved seal. However, when using the total pressure inlet boundary condition, convergence problems were encountered due to the flow recirculation (trying to exit the domain) as shown in Figure 18. This problem was alleviated by using an inlet boundary condition (velocity specified) yielding the desired mass flow. The same exit pressure boundary condition is used; therefore, total pressure drop across the seal is predicted rather than leakage. To simulate the radial inlet supply to this upstream cavity, the radial velocity is assumed to be equal to the axial velocity and is directed inwards (V=-U). This boundary condition smooths out the upstream flow field and causes a large vortex in the first domain as shown in Figure 19. The swirl velocity in this inlet region is accelerated by the Couette action of the rotor and

steadily increases as the flow approaches the first seal land shown in Figure 20 (10,200 rpm). The swirl velocity at 24,600 rpm is shown in Figure 21 and is normalized to the same ratio of rotor surface speed as Figure 20. This plot shows the swirl velocity to develop faster and causes an increase in the inlet swirl ratio (Wrat) at the seal entrance.

The static pressure distribution in both the upstream section and the first seal land is plotted in Figure 22. Some of the drop is due to the increase in velocity while the remainder is due to inertial and viscous total pressure losses. Using the inlet pressure drop (ΔP) and mean axial velocity, the inlet loss factor may be calculated. The values for inlet loss factor and swirl ratio are summarized below:

Speed (rpm)	ζ	Wrat
10200	0.63	0.28
24600	0.7	0.36

These values were used in the total pressure boundary condition with the Fine Grid-1 mesh (without upstream region). Furthermore, the averaged values for k and ε were obtained from the 2D analysis and used in the 3D calculations as well. Figures 23 and 24 show how the axial and circumferential velocity distributions develop from the entrance to exit of the first seal land. Bulk flow is a reasonable assumption in this plain annular section. The axial and circumferential profiles in the center of the cavity resemble the bulk flow/pure vortex assumption used by the 3 control volume analysis. Table 6 compares the prediction of force coefficients and leakage with the experiment. The inlet swirl still appears to be under predicted indicated by the cross-coupled stiffness. The damping prediction has improved. The leakage is slightly less. The prediction at 24,600 under-predicts the direct stiffness prediction but much improved prediction of cross-coupled stiffness compared to the 3-CV method. The reason for CFD's under-prediction of the damping and inertia terms is unclear. Including the upstream fluid mass in the 3D calculation would perhaps improve the inertia prediction.

While this second analysis procedure did not yield as good as prediction as the first analysis, it is still the preferred technique in the absence of test data. The axisymmetric analysis may be obtained with low computational effort and eliminates much of the question of boundary conditions.

Conclusion

The general purpose, 3D seal code SCISEAL is validated against test data for a high speed, high pressure grooved liquid annular seal. The calculated cross-coupled stiffness is a strong function of the inlet boundary condition (ie. inlet swirl). In the absence of quality test data, an axisymmetric analysis has provide the inlet boundary conditions used in the 3D analysis. However, the swirl entering the seal appears still to be under predicted. The k-ε turbulence model struggles with swirling type flows and may be one of the sources of error.

Future work includes validation of other speeds and pressures. In addition, comparisons between the performance of different turbulence models will be performed.

Acknowledgement

The authors would like to thank Dr. Mahesh Athavale at CFD Research Corp. for support and expertise in the use of SCISEAL. Thanks goes to NASA Lewis Research Center for providing the funding to develop SCISEAL under the Earth-to-Orbit Propulsion program.

REFERENCES

Arghir, M., Frene, J., 1997, "Rotordynamic Coefficients of Circumferentially-Grooved Liquid Seals Using the Average Navier-Stokes Equations," *Journal of Tribilogy*, **119**, pp. 556-567.

Athavale, M.M., Przekwas, A.J., Hendricks, R.C., Liang, A., 1994, "SCISEAL: A 3D CFD Code for Accurate Analysis of Fluid Flow and Forces in Seals," Advance ETO Propulsion Conference, May, 1994.

Black, H., 1969, "Effects of Hydraulic Forces on Annular Pressure Seals on the Vibrations of Centrifugal Pump Rotors," *Journal of Mechanical Engineering Science*, **11** (2), pp. 206-203.

Childs, D., 1983, "Dynamic Analysis of Turbulent Annular Seals Based on Hirs' Lubrication Equation, " *Journal of Lubrication Technology*, **105**, pp. 437-444.

Dietzen, F., and Nordmann, R., 1986, "Calculating Rotordynamic Coefficients of Seals by Finite Difference Techniques," Rotordynamic Instability Problems in High Performance Turbomachinery, NASA CP No. 3026, proceedings of a workshop held at Texas A & M University, pp. 197-210.

Florjancic, S., 1990, "Annular Seals of High Energy Centrifugal Pumps: A New Theory and Full Scale Measurement of Rotordynamic Coefficients and Hydraulic Friction Factors," dissertation, Swiss Federal Institute of Technology, Zürich, Switzerland.

Marquette, O.R., 1995, "Experimental vs. Theoretical Comparisons of the Static and Dynamic Characteristics of One Smooth and Two Grooved Liquid Annular Seals with L/D of 0.457," Turbomachinery Research Consortium Report, TL-SEAL-5-95, Texas A & M University.

Rhode, D.L., Hensel, S.J., and Guidry, M.J., 1992, "Three-Dimensional Computations of Rotordynamic Force Distribution in a Labyrinth Seal," *Tribology Transactions*, Vol. 36, **3**, pp. 461-469.

INTRODUCTION

- **SCISEAL** (Athavale, et al., 1994)
  - Developed by CFD Research Corp. under NASA contract
  - General 3D CFD
  - Stationary/Rotating Frames of Reference
  - Cylindrical, Body Fitted, Structured Grid
  - Compressible / Incompressible
  - Advanced Turbulence Models
  - Multi-Domain
  - Fully Integrated to Pre/Post Processors (GEOM & VIEW)

- **Solution Procedure**
  - Integrates Pressure and Shear Stresses
  for each Whirl Frequency Ratio (WFR)
  of 3-D Eccentric Mesh
  - Coordinate System Attached to Whirling Rotor
  - Impedance Forces (Normal and Cross-coupled)
  Found for Multiple Whirl Speeds
  - Rotordynamic Force Coefficients Determined by
  Fitting 2nd Order Curvefit to Impedance Forces:

$$\bar{F}_n = \frac{F_n}{\epsilon} = -K - c\omega + M\omega^2$$

$$\bar{F}_t = \frac{F_t}{\epsilon} = k - C\omega - m\omega^2$$

where, ϵ = eccentricity
K, C, M = direct stiffness, damping, mass
k, c, m = cross-coupled stiffness, damping, mass

THEORY

- **Reynolds Averaged Navier-Stokes Equations:**

$$U_j \frac{\partial U_i}{\partial x_j} = \frac{1}{\rho}\left(-P\delta_{ij} + 2\mu S_{ij} - \overline{\rho u_i u_j}\right)$$

- **Eddy Viscosity Concept**

$$-\overline{\rho u_i u_j} = \mu_t\left(\frac{\partial U_i}{\partial x_j} + \frac{\partial U_j}{\partial x_i} - \frac{2}{3}\frac{\partial U_m}{\partial x_m}\delta_{ij}\right) - \frac{2}{3}\rho k \delta_{ij}$$

$$\mu_t = \rho C_\mu \frac{k^2}{\varepsilon}$$

$$k = \frac{1}{2}\overline{u_k u_k}$$

- **k-ε Turbulence Model**

$$\frac{\partial k}{\partial t} + U_i \frac{\partial k}{\partial x_i} = \frac{\partial}{\partial x_i}\left(\frac{\nu_t}{\sigma_k}\frac{\partial k}{\partial x_i}\right) + P + G - \varepsilon$$

$$\frac{\partial \varepsilon}{\partial t} + U_i \frac{\partial \varepsilon}{\partial x_i} = \frac{\partial}{\partial x_i}\left(\frac{\nu_t}{\sigma_\varepsilon}\frac{\partial \varepsilon}{\partial x_i}\right) + C_{1\varepsilon}\frac{\varepsilon}{k}(P+G)\left(1 + C_{3\varepsilon}R_f\right) - C_{2\varepsilon}\frac{\varepsilon^2}{k}$$

- **Log Law of the Wall**

$$u^+ = y^+ \qquad \text{for } y^+ < 11.5$$

$$u^+ = \frac{u_\tau}{K}\ln(E y^+) \qquad \text{for } y^+ > 11.5$$

- 2-Layer Turbulence Model Used
(Std. k-ε, w/ inner layer algebraic expression for ε)

OTHER SEAL ANALYSIS TECHNIQUES

- **Bulk-Flow Techniques**
  - Assume Uniform Velocity Distributions for Steady Analysis
  - Assumes Harmonic Variation of Flow Variables in Circumferential Direction for Dynamic Analysis
  - Uses Empirical Turbulent Wall Shear Stress Relations (Blasius, Moody)
  - Efficient Solution
  - Accurate for Plain Annular Seals
  - Poor in Presence of Recirculations (labyrinth, grooved seals)
  - Black (1969), Childs (1983)

- **3 Control-Volume Technique**
  - Couples Two Bulk Flow and a Single Vortex CV's
  - Empirical Jet Shear Stress at Interface
  - Reasonable Prediction for Square Groove Cavities
  - Florjancic (1990), Marquette (1995)

- **OTHER CFD TECHNIQUES**
  - Solve Dynamic Flow Field Using Coordinate Trans.
  - Casts Eccentric Rotor into 2D Axisymmetric Coord. System
  - Dietzen and Nordman (1986), Arghir and Frene (1997)
  - Efficient, But Does Not Capture Variation of k and ε Around Circumference
  - Cannot Model Non-Axisym. Geometries (ie. Swirl Breaks)

Mesh Density Description for Grooved Liquid Seal

	Land	Groove	Circum.	# Nodes
Coarse Grid-2	9 X 7	15 X 17	21	45864
Coarse Grid-1	9 X 7	15 X 17	31	67704
Medium Grid	9 X 7	25 X 23	31	140399
Fine Grid-1	9 X 11	25 X 27	31	176452
Fine Grid-2	15 X 15	30 X 39	31	309690

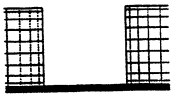

Coarse Grid 1 & 2

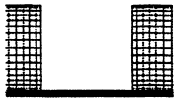

Medium Grid

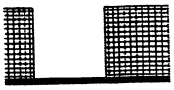

Fine Grid-1

Fine Grid-2

Table 1 Mesh Density Description for Grooved Liquid Seal

Force Coefficients for Grooved Liquid Seal

10,200 rpm, 4.14 MPa, Medium Grid, Wrat=0.45, Ploss=0.1

	Computation	Experiment	3 Control Vol.
Kxx/Kyy (KN/m)	19.9	-5	-130
Kxy/-Kyx (KN/m)	421	740	99.8
Cxx/Cyy (KN-s/m)	2.45	4.81	4.59
Cxy/-Cyx (KN-s/m)	1.57	3.63	3.16
Mxx/Myy (kg)	1.43	5.19	3.59
Mxy/-Myx (kg)	0.46	-	-
WFR (Kxy / Cxx w)	0.16	0.14	0.02
Leakage (l/s)	0.72	0.82	0.82

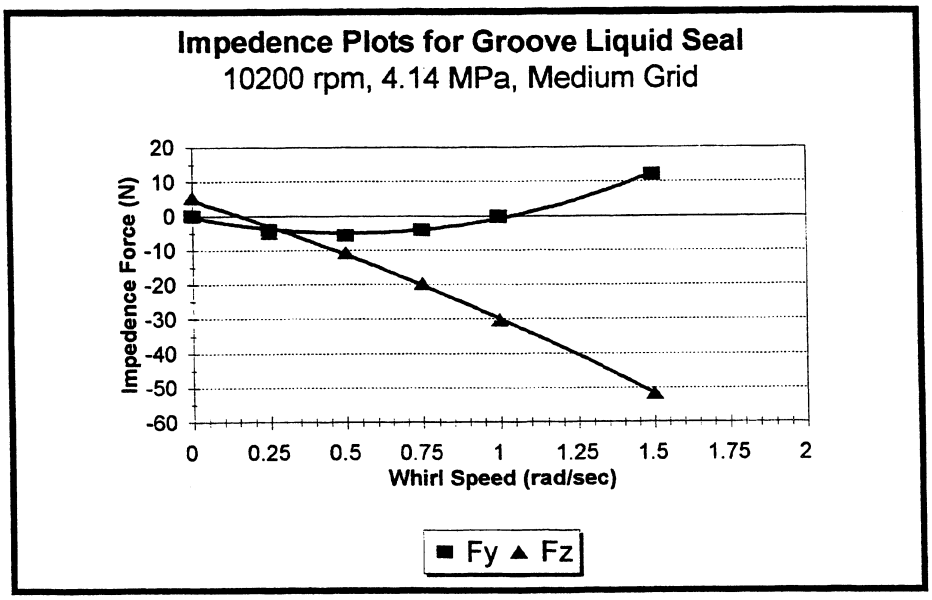

Table 2 Force Coefficients - Medium Grid, 10200 rpm, Wrat=0.45, Ploss=0.1

Force Coefficients for Grooved Liquid Seal

24,600 rpm, 6.20 MPa, Medium Grid, Wrat=0.45, Ploss=0.1

	Computation	Experiment	3 Control Vol.
Kxx/Kyy (KN/m)	-949	-2490	-3560
Kxy/-Kyx (KN/m)	3740	3790	350
Cxx/Cyy (KN-s/m)	3.99	6.78	6.96
Cxy/-Cyx (KN-s/m)	2.83	8.84	7.21
Mxx/Myy (kg)	1.18	5.14	3.22
Mxy/-Myx (kg)	0.30	-	-
WFR (Kxy / Cxx w)	0.36	0.22	0.02
Leakage (l/s)	0.82	0.97	0.897

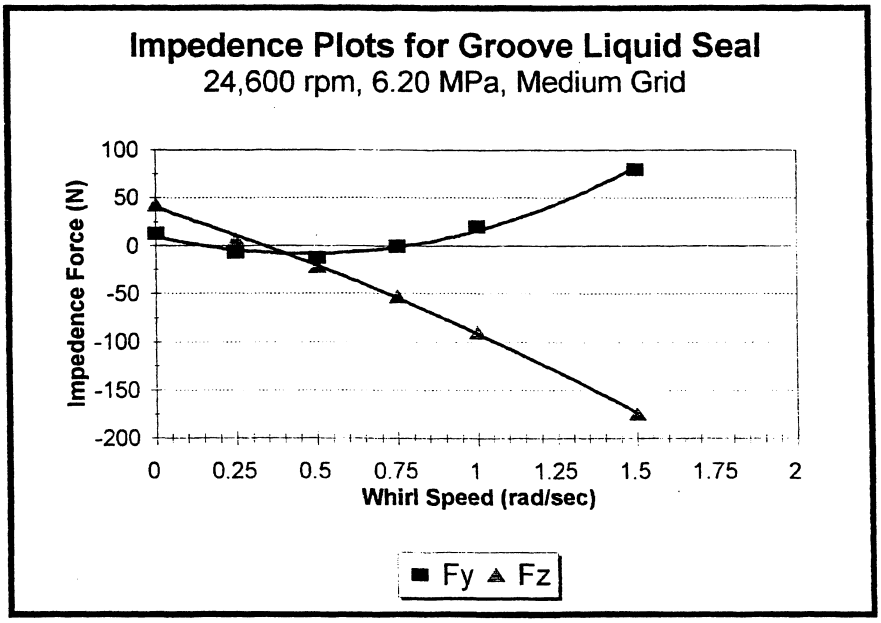

Table 3 Force Coefficients - Medium Grid, 24600 rpm, Wrat=0.45, Ploss=0.1

Mesh Density Study for Grooved Liquid Seal

10,200 rpm, 4.14 MPa, Wrat=0.45, Ploss=0.1

	Kxx/Kyy	Kxy/-Kyx	Leakage	# Nodes
Coarse Grid-2	302	564	0.73	45864
Coarse Grid-1	176	528	0.74	67704
Medium Grid	19.9	421	0.72	140399
Fine Grid-1	5.69	1026	0.72	171027
Fine Grid-2	174	981	0.71	309690
Experiment	-5.00	740	0.82	

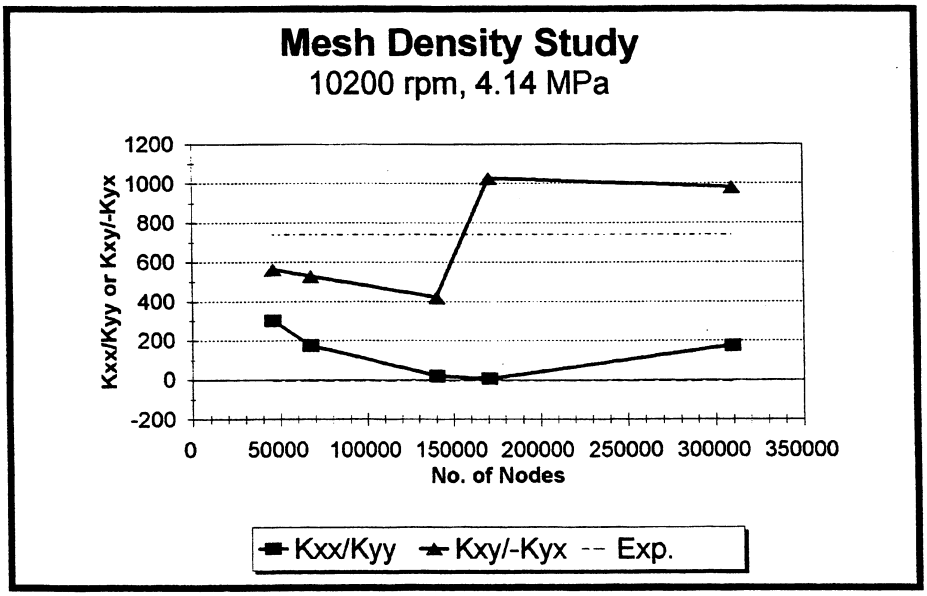

Table 4 Mesh Density Study - Stiffness Coefficients and Leakage
10200 rpm, Wrat=0.45, Ploss=0.1

Mesh Density Study for Grooved Liquid Seal

10,200 rpm, 4.14 MPa, Wrat=0.45, Ploss=0.1

	Cxx/Cyy	Cxy/-Cyx	Mxx	# Nodes
Coarse Grid-2	2.68	1.28	1.08	45864
Coarse Grid-1	2.6	1.61	1.49	67704
Medium Grid	2.45	1.57	1.43	140399
Experiment	4.81	3.63	5.19	

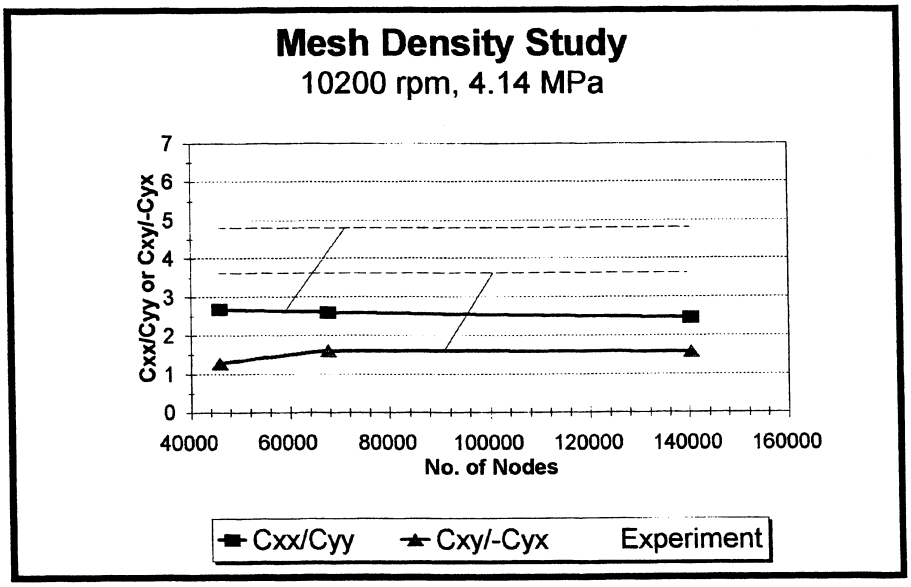

Table 5 Mesh Density Study - Damping and Inertia Coefficients
10200 rpm, Wrat=0.45, Ploss=0.1

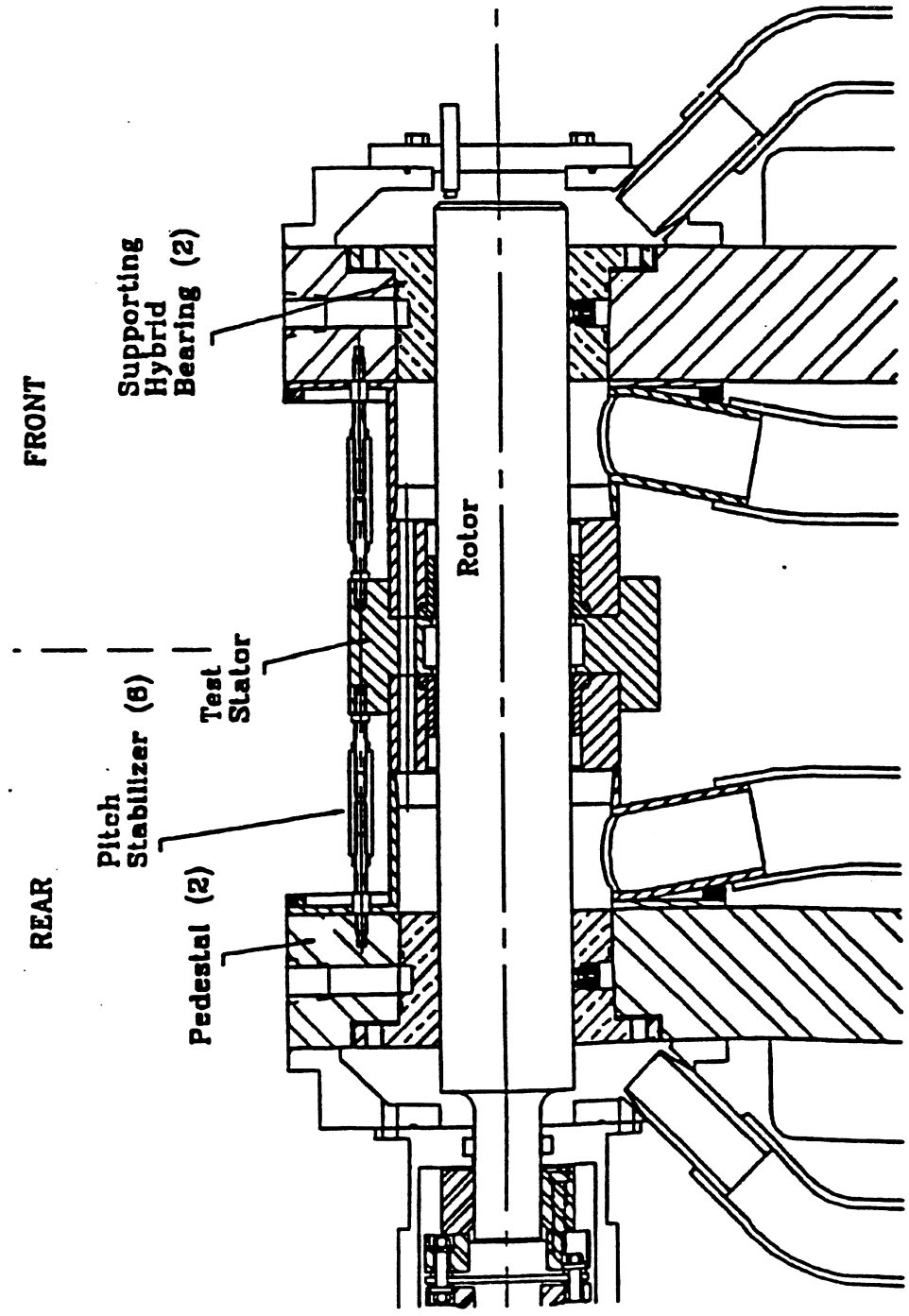

Figure 1 High Speed Seal Test Rig
(Courtesy of Marquette and Childs, 1995)

Fine Grid, 11 x 9 land, 27 x 25 groove

Rshaft = 38.15 mm, Clear.=0.11 mm

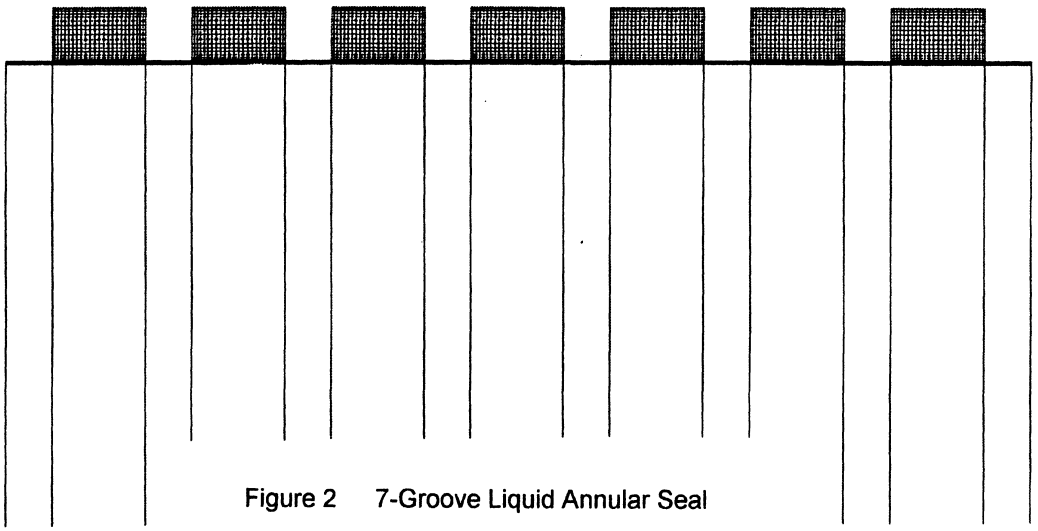

Figure 2 7-Groove Liquid Annular Seal

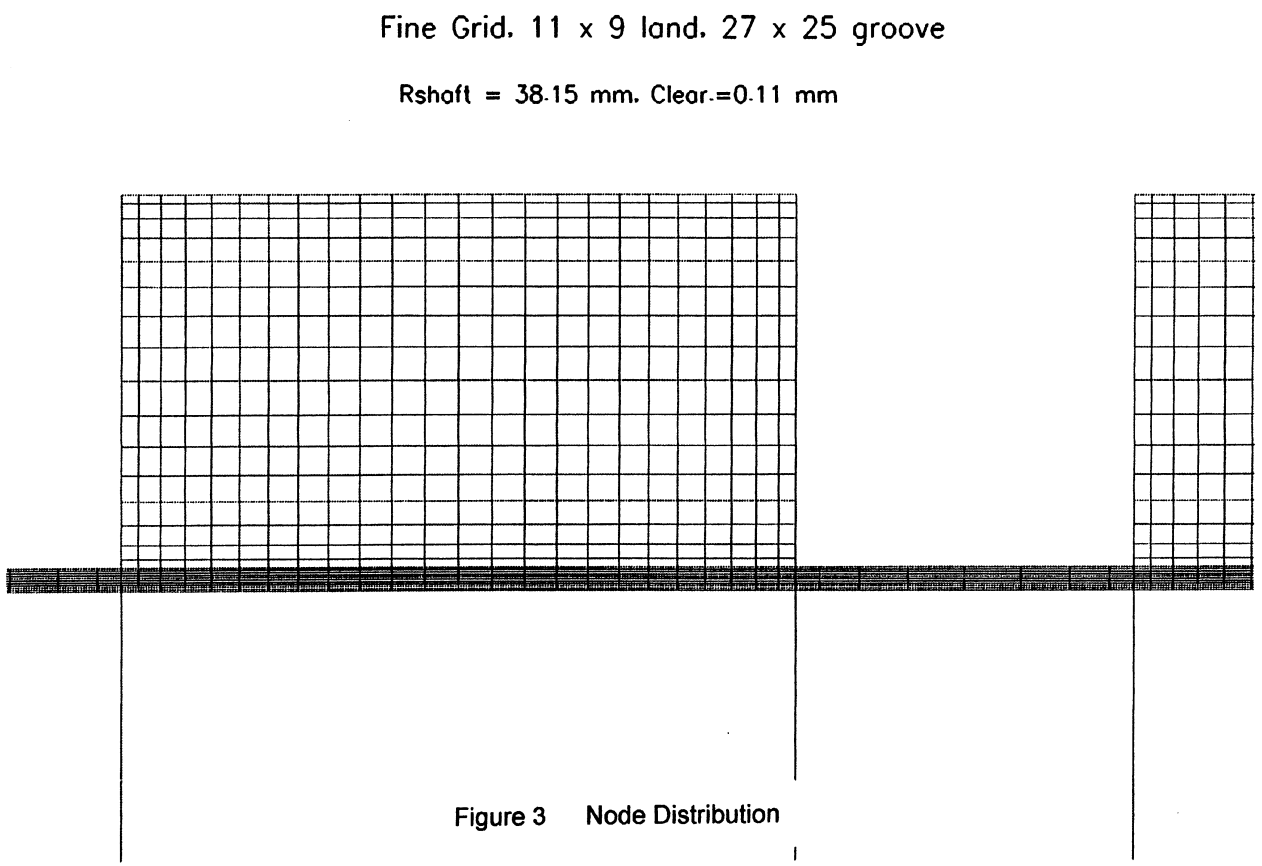

Figure 3 Node Distribution

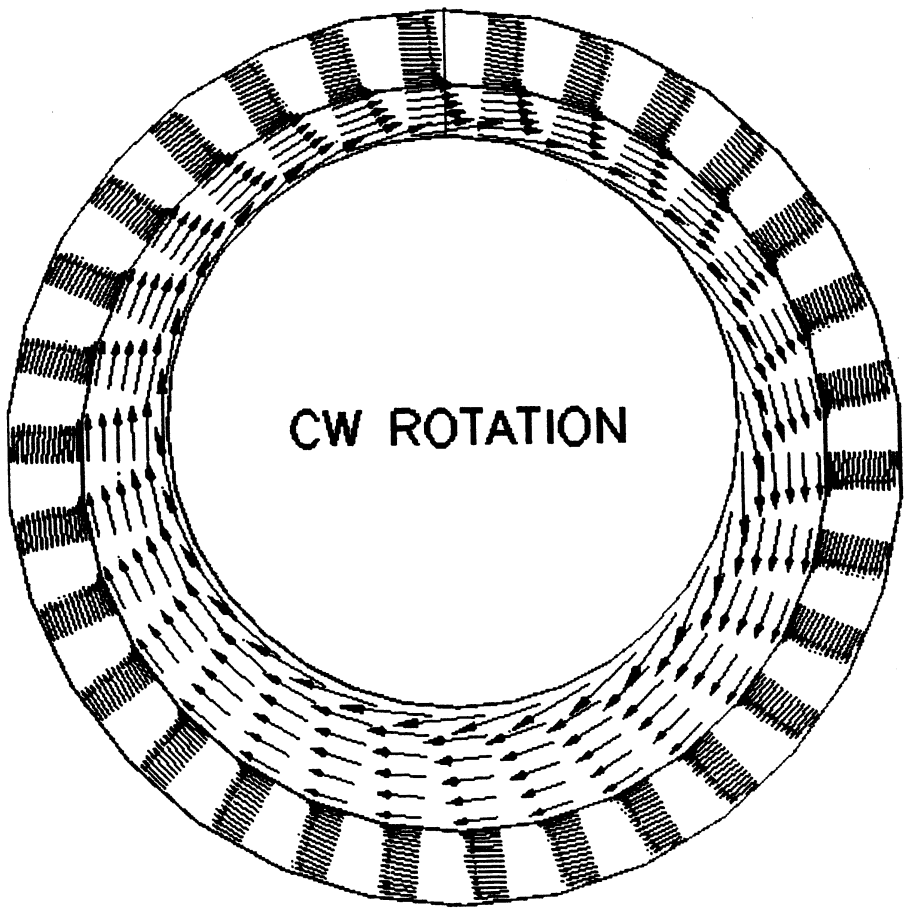

Figure 4 Circumferential Velocity Distribution

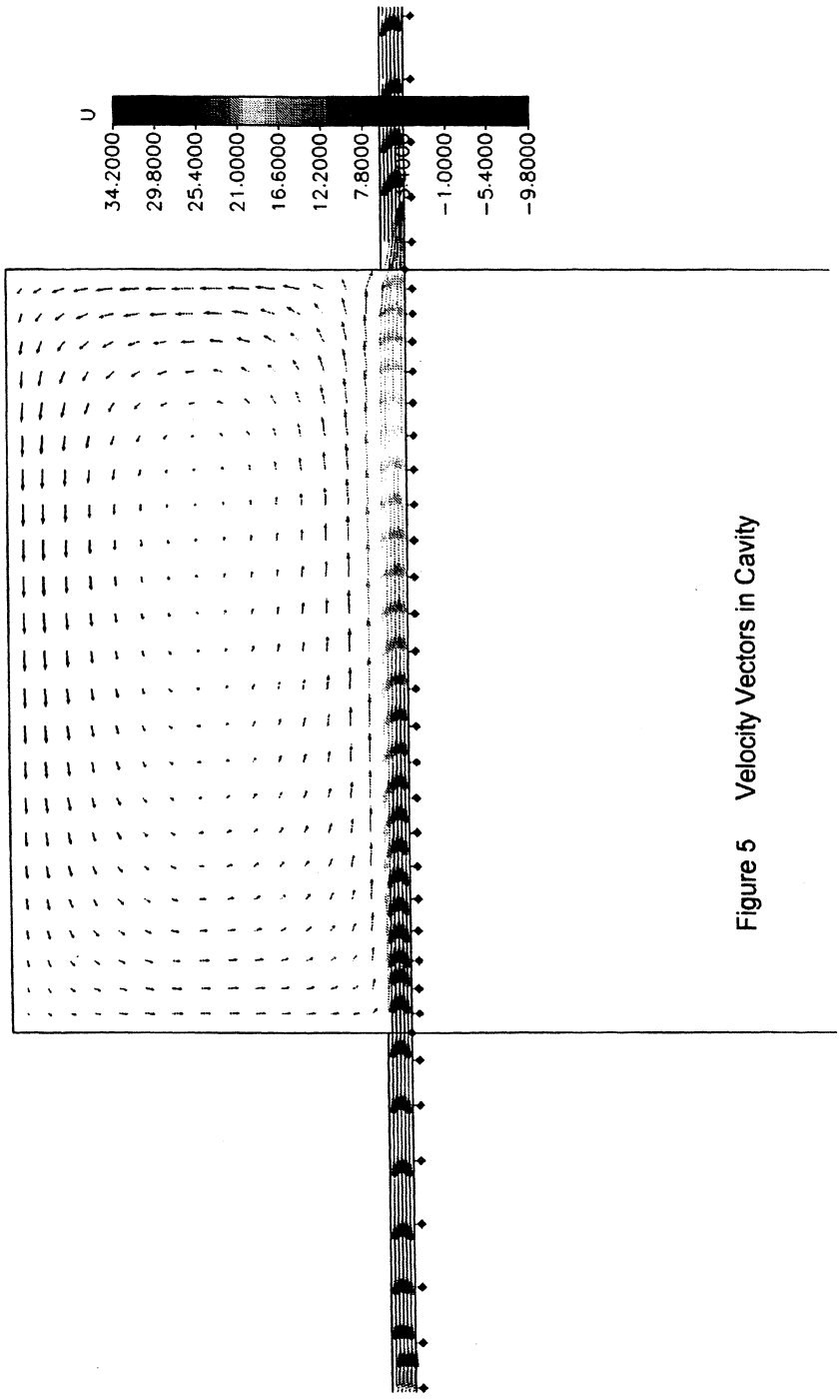

Figure 5 Velocity Vectors in Cavity

Figure 6 Velocity Vectors Entering Seal Land

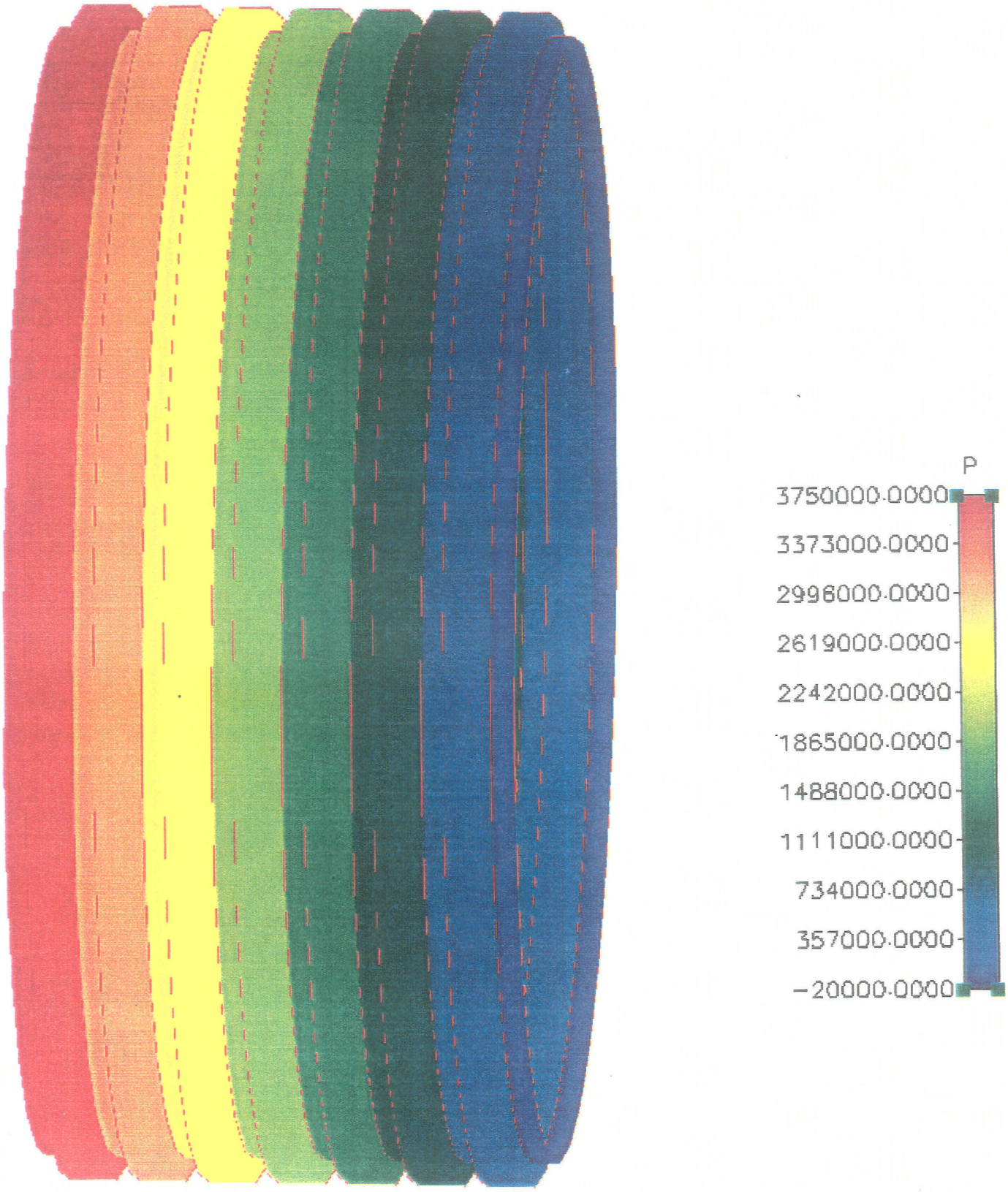

Figure 7 Static Pressure Drop Through Seal

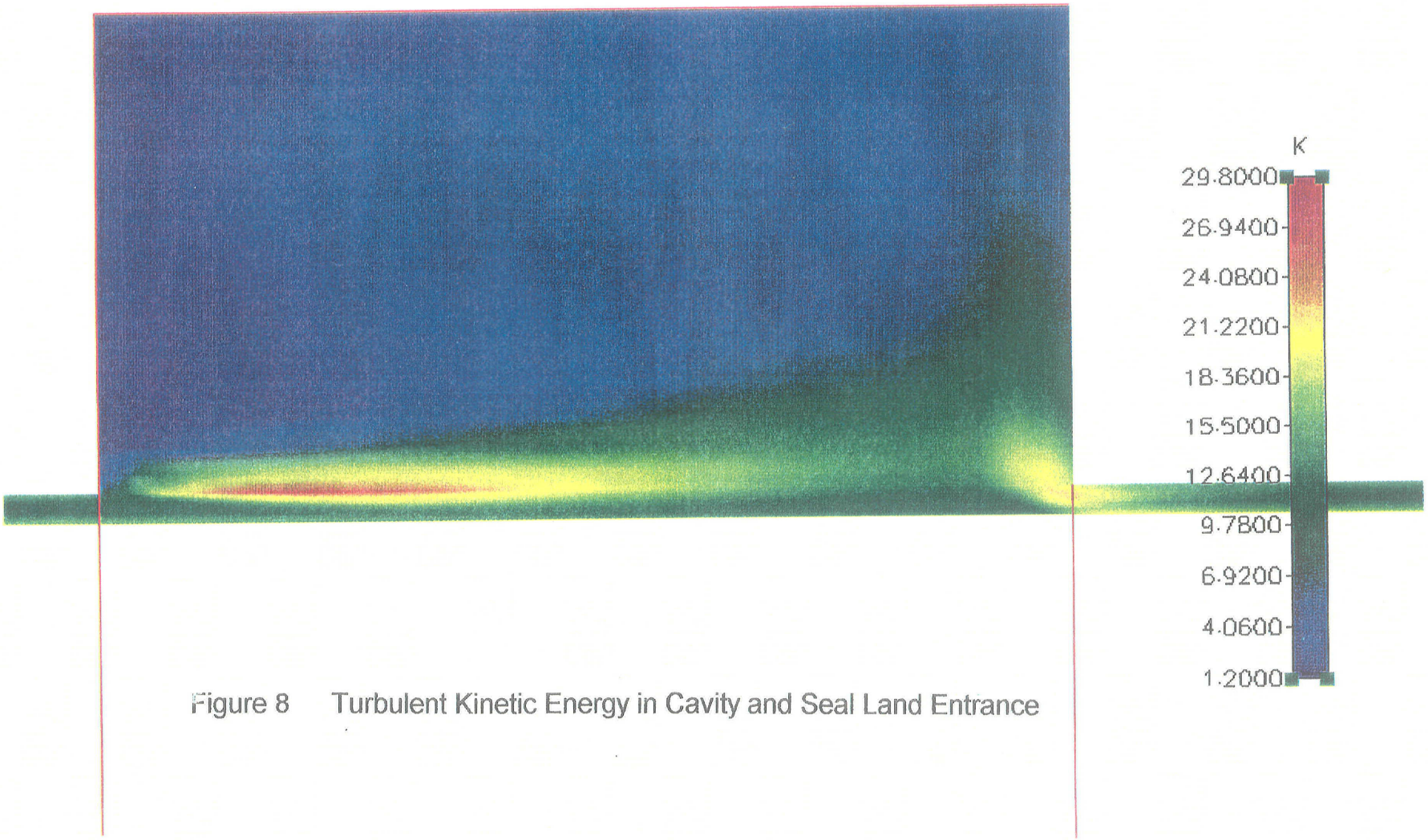

Figure 8 Turbulent Kinetic Energy in Cavity and Seal Land Entrance

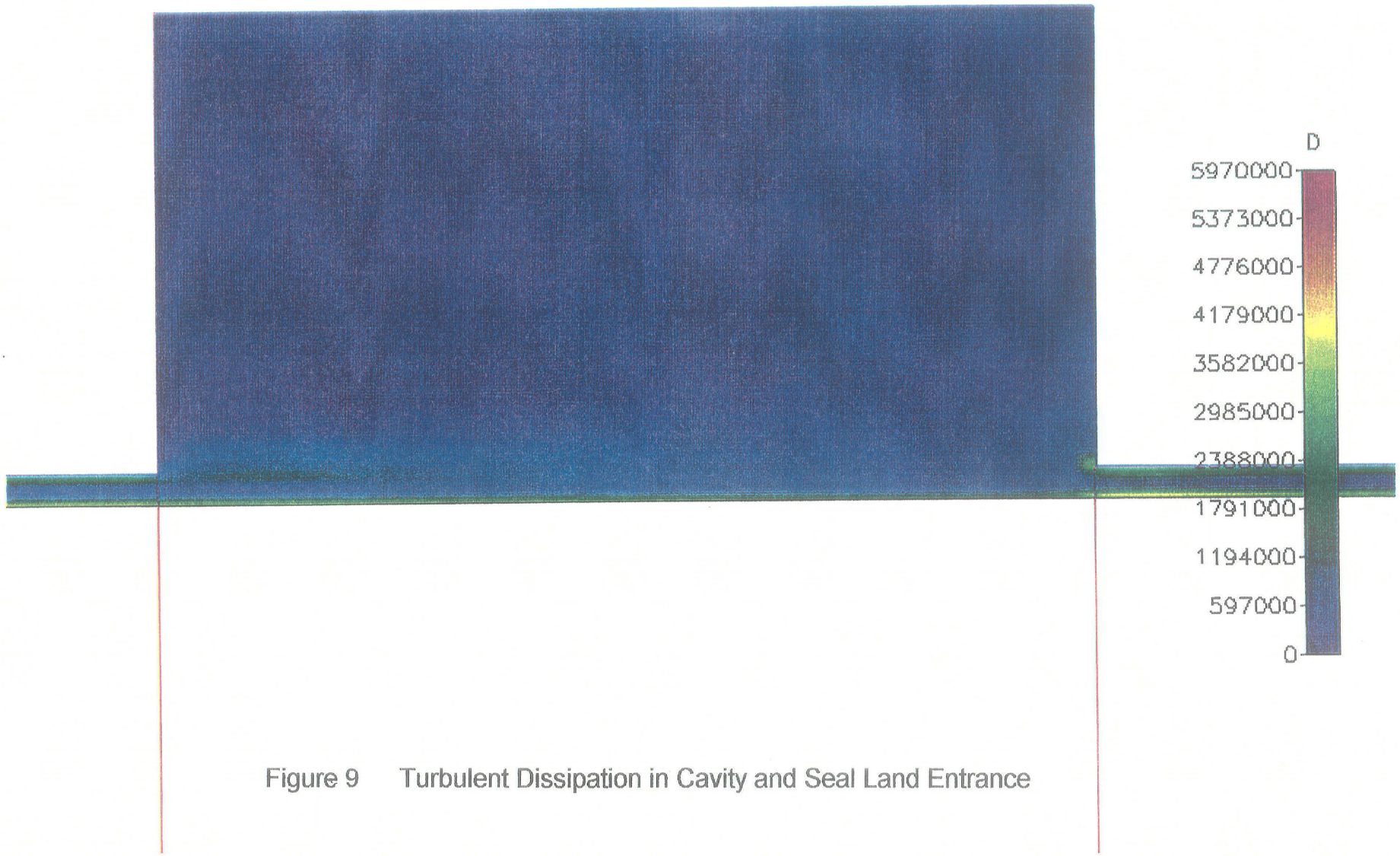

Figure 9 Turbulent Dissipation in Cavity and Seal Land Entrance

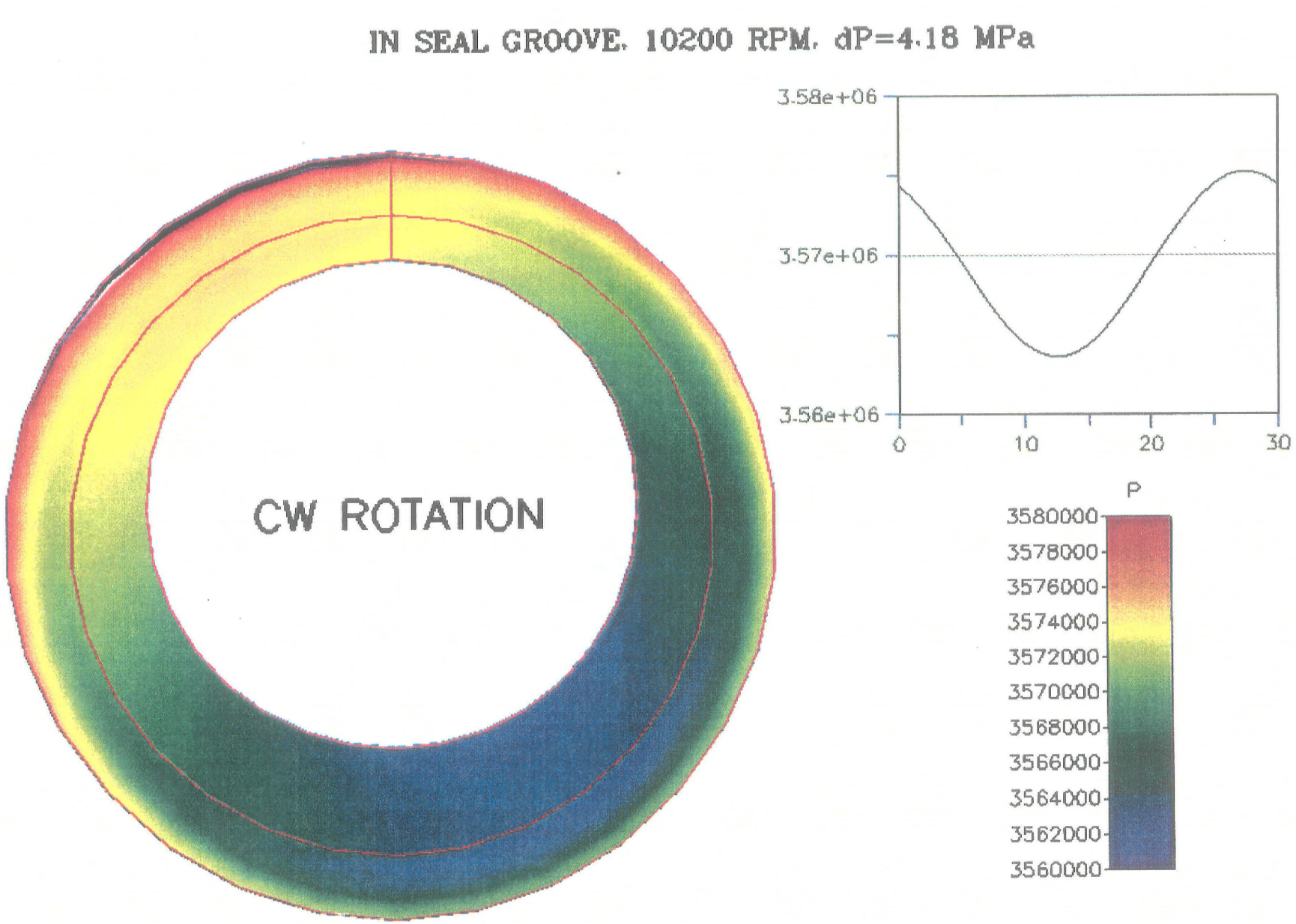

Figure 10 Circumferential Pressure Distribution, WFR=0.0

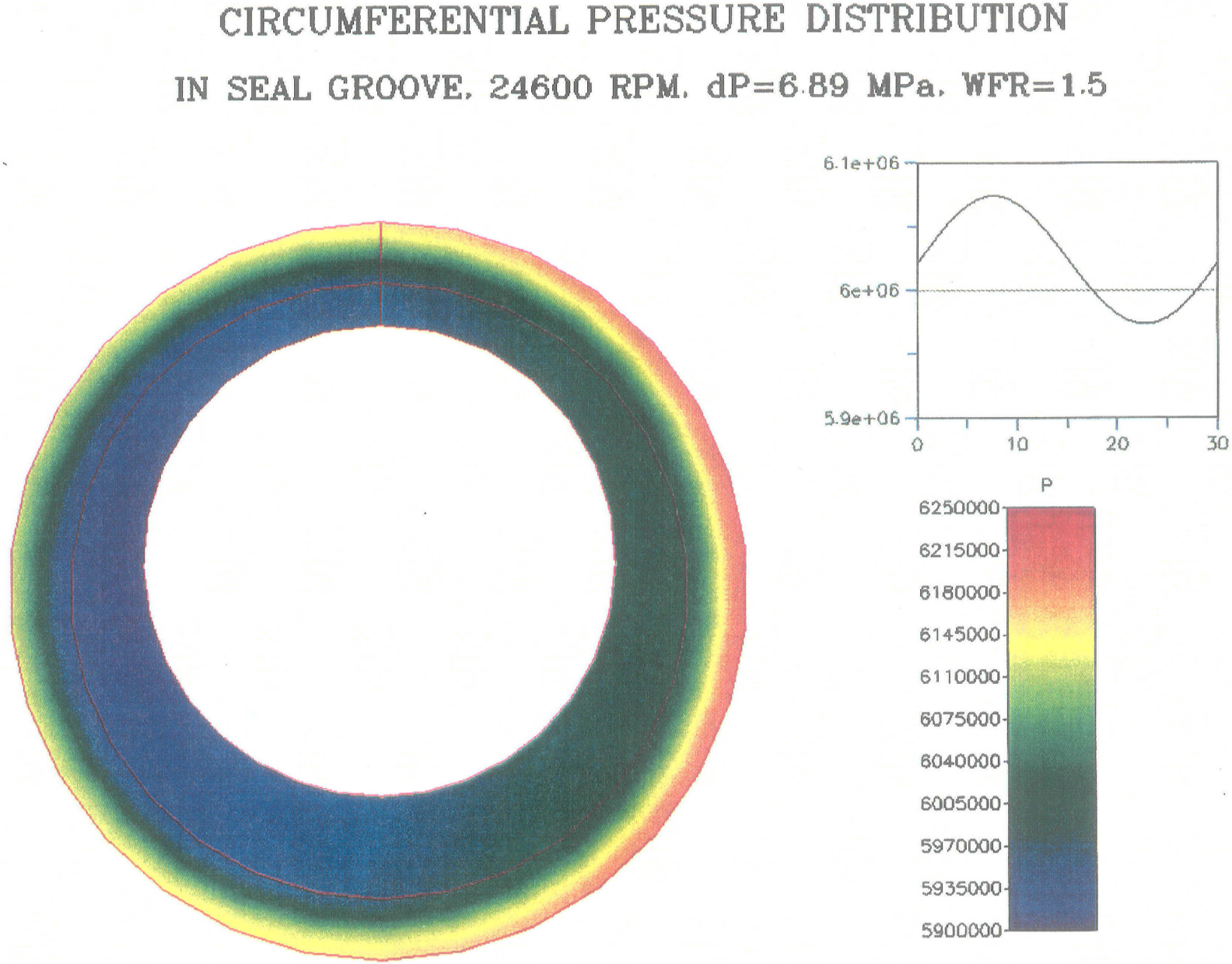

Figure 11 Circumferential Pressure Distribution, WFR=1.5

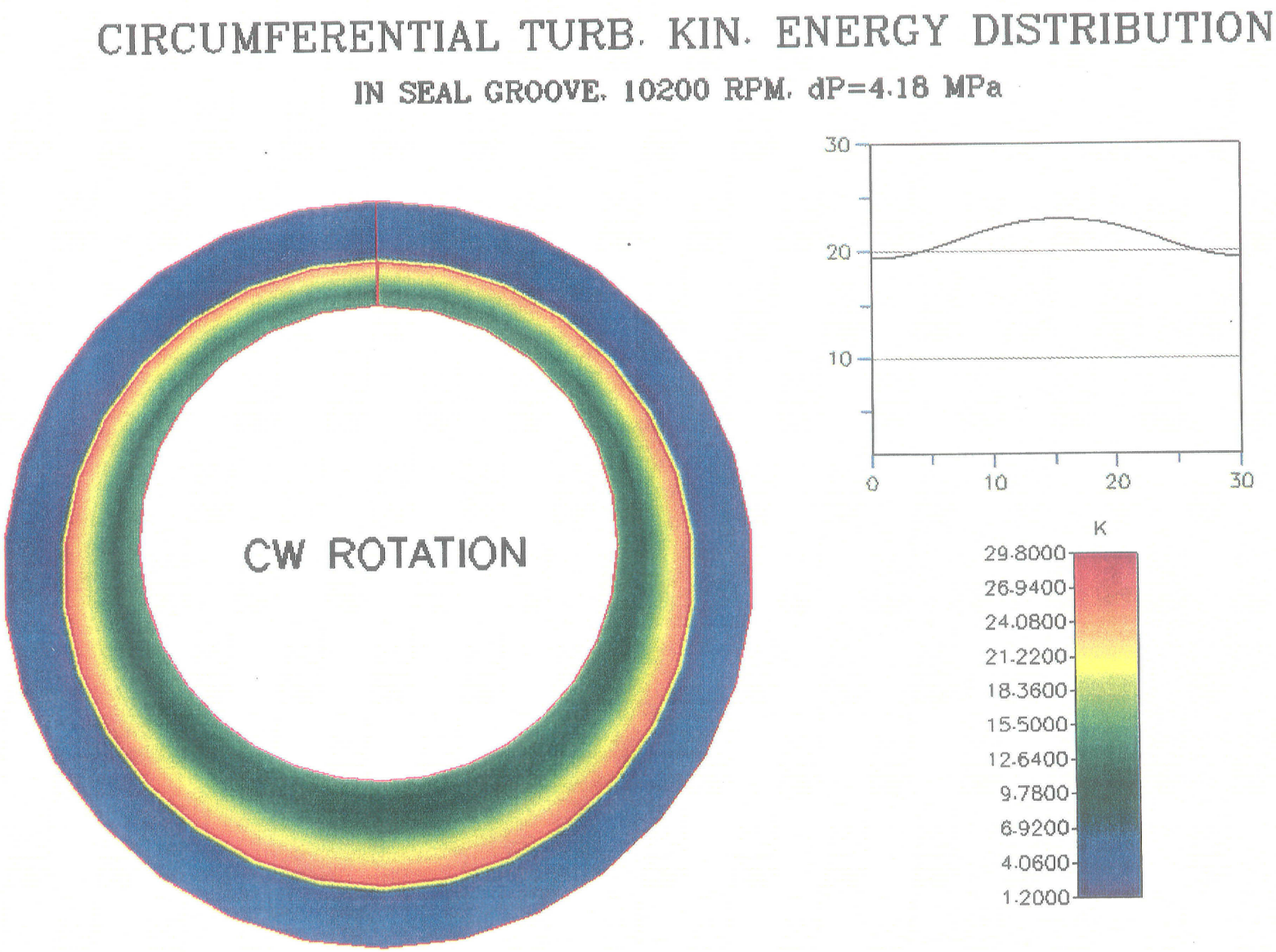

Figure 12 Circumferential Turbulent Kinetic Energy Distribution

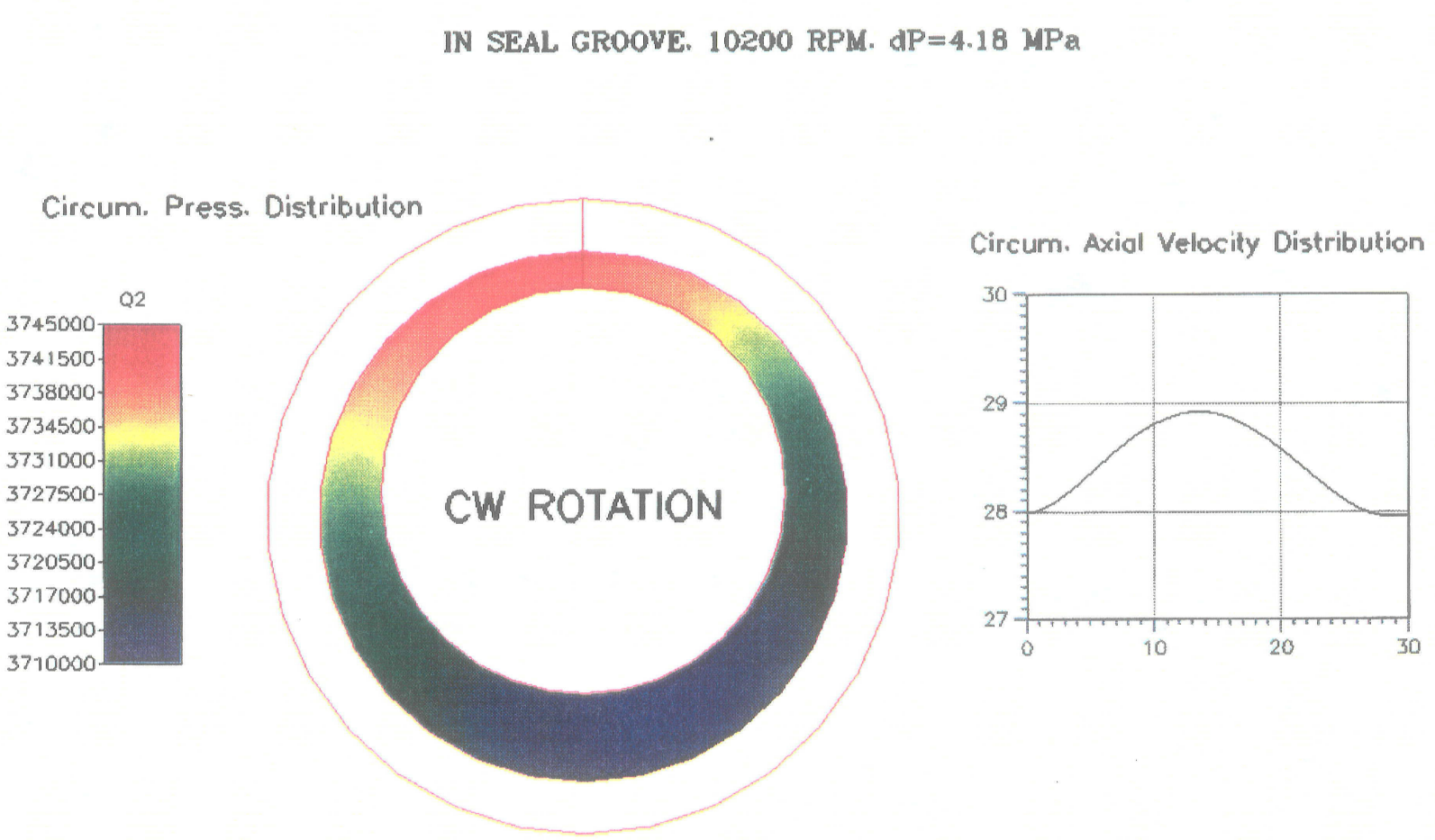

Figure 13 Velocity and Static Pressure Distribution at Entrance (Total-P BC)

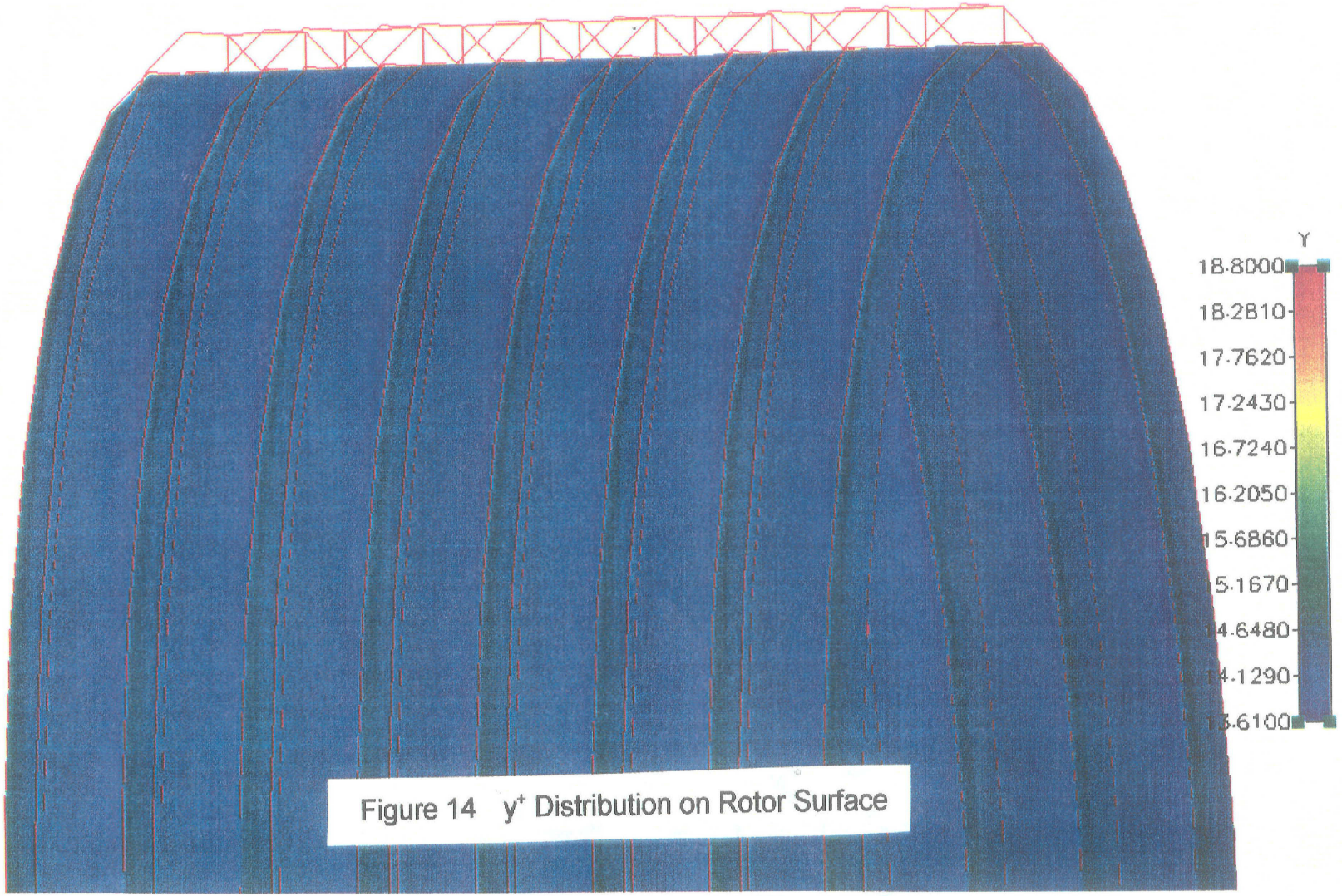

Figure 14 y^+ Distribution on Rotor Surface

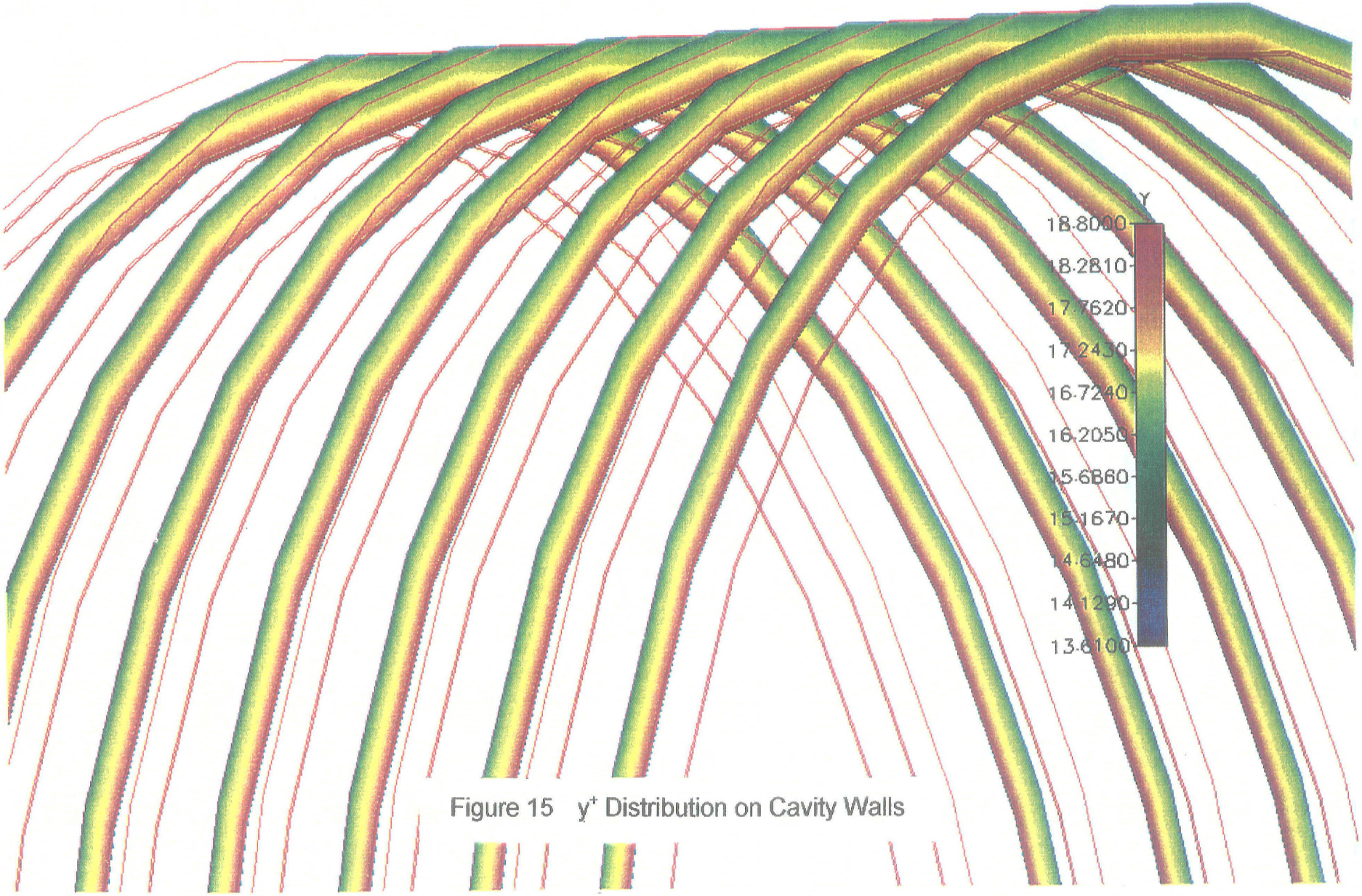

Figure 15 y^+ Distribution on Cavity Walls

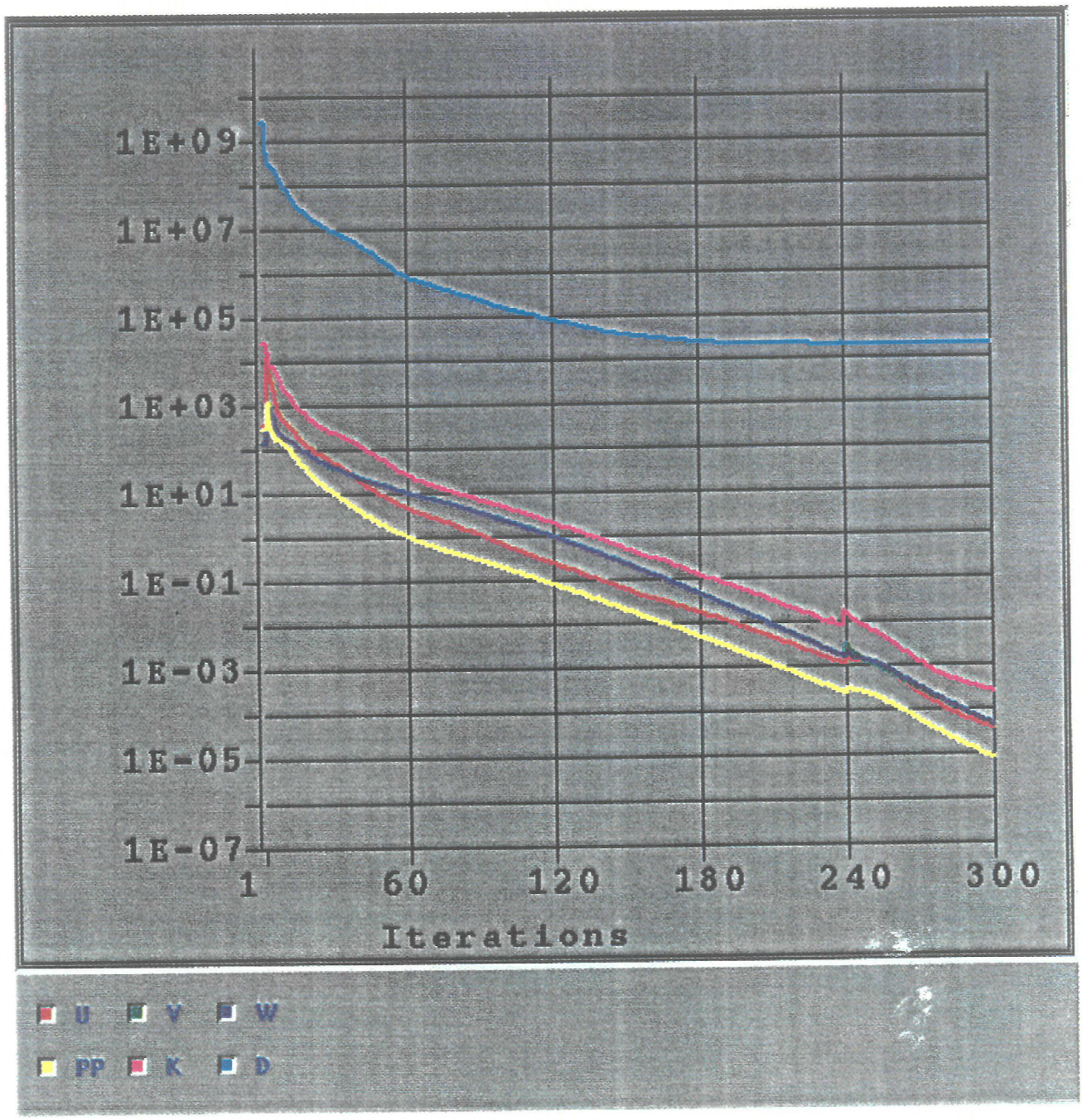

Figure 16 Residual Decay - Coarse Grid-1

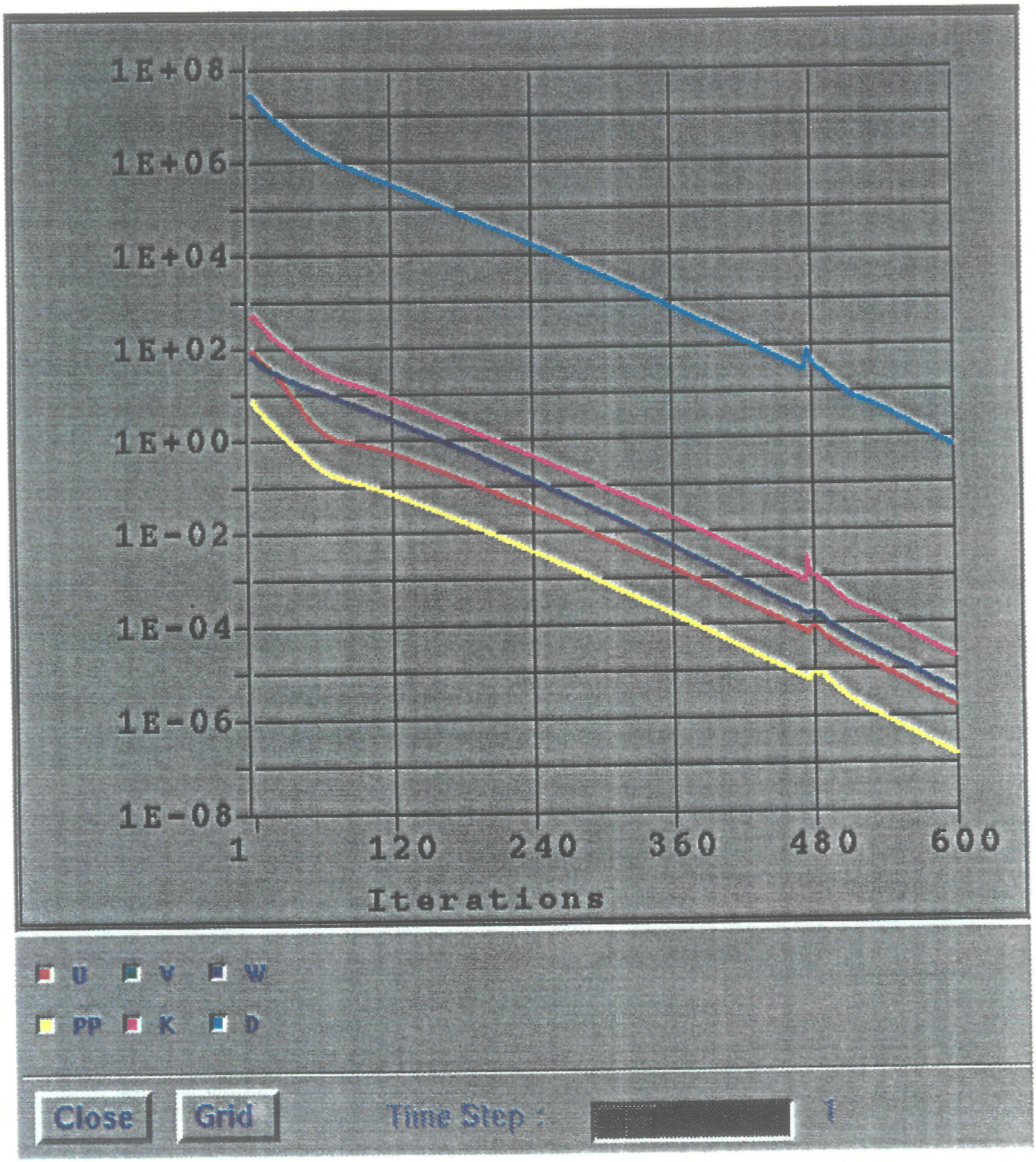

Figure 17 Residual Decay - Medium Grid

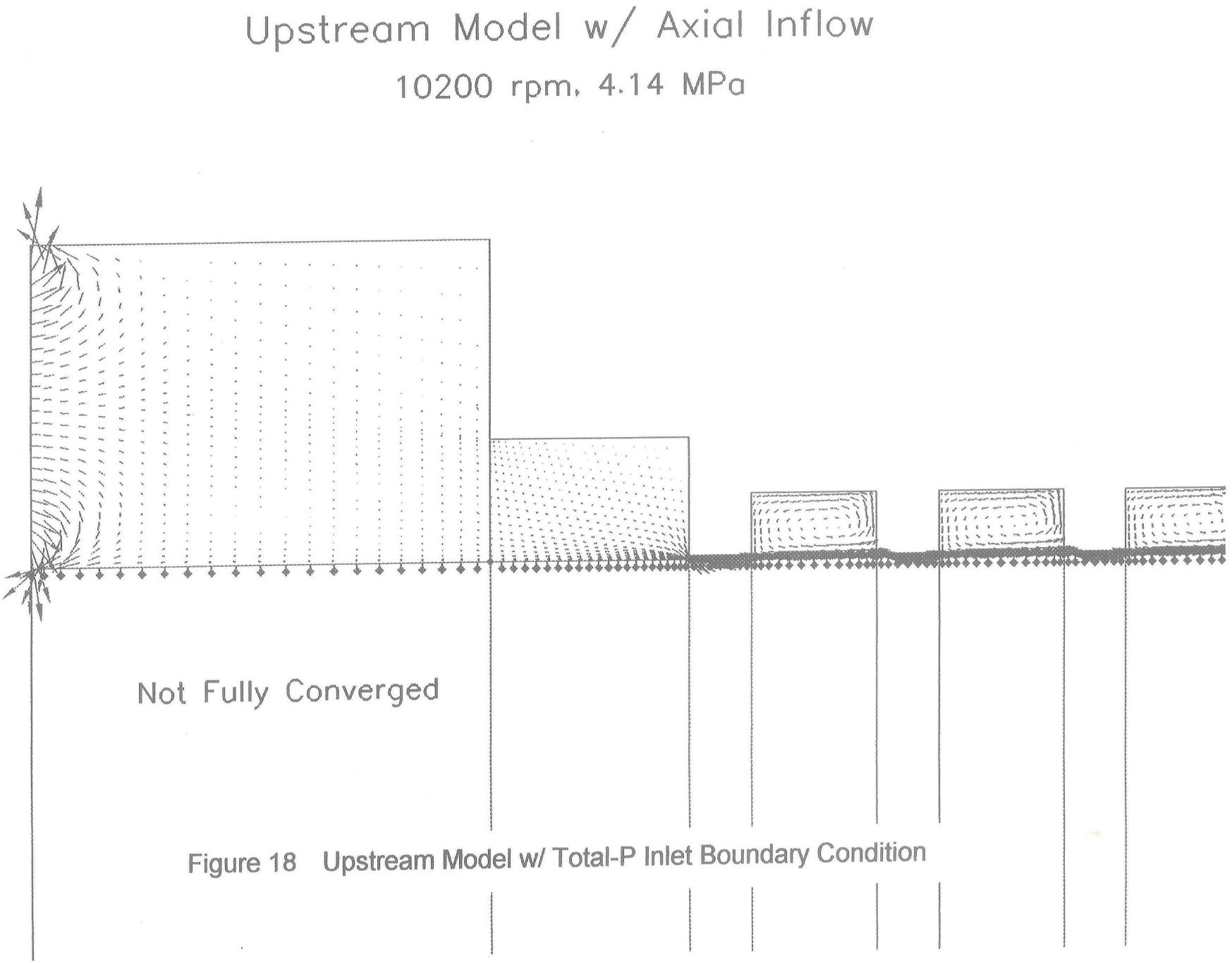

Figure 18 Upstream Model w/ Total-P Inlet Boundary Condition

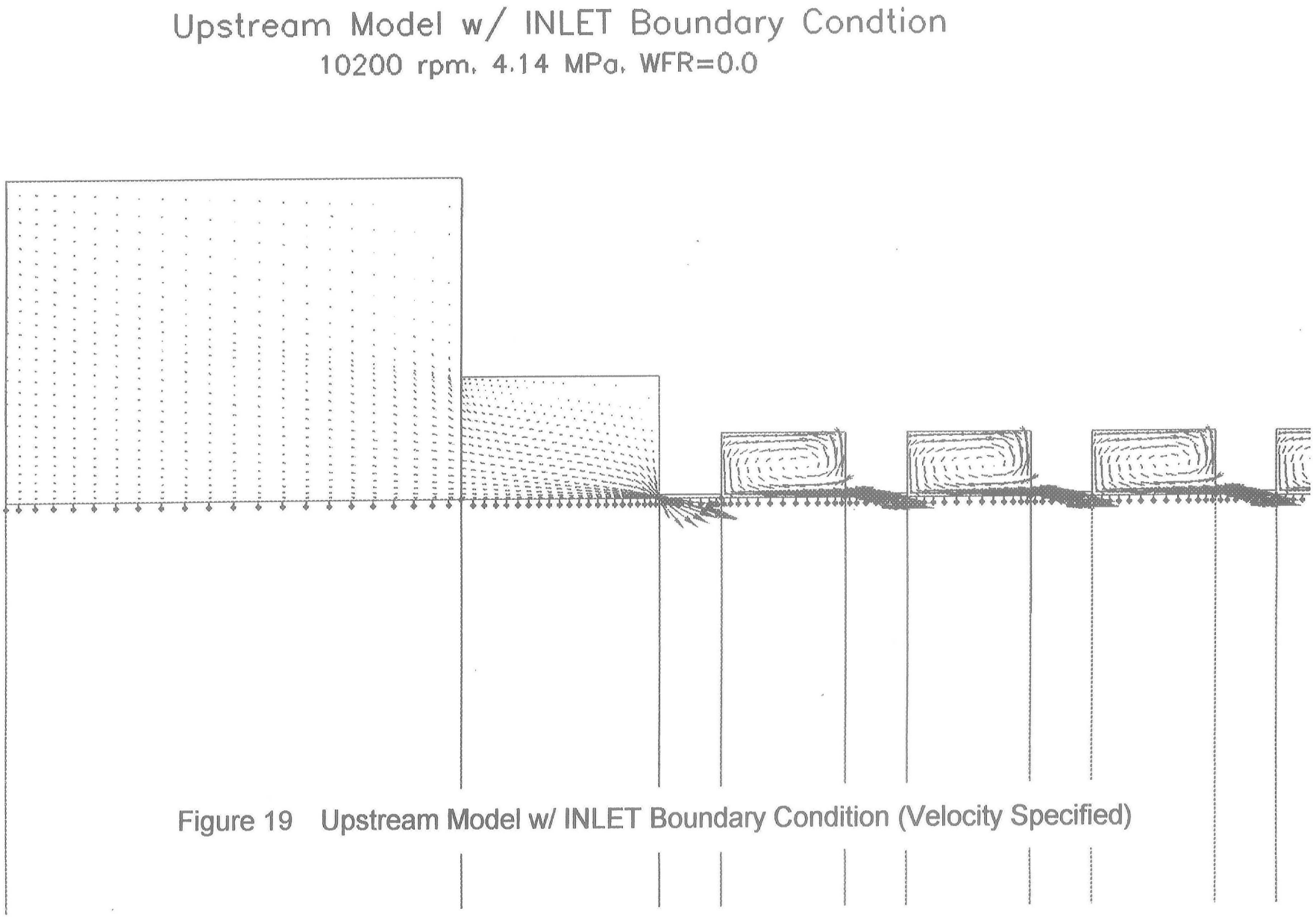

Figure 19 Upstream Model w/ INLET Boundary Condition (Velocity Specified)

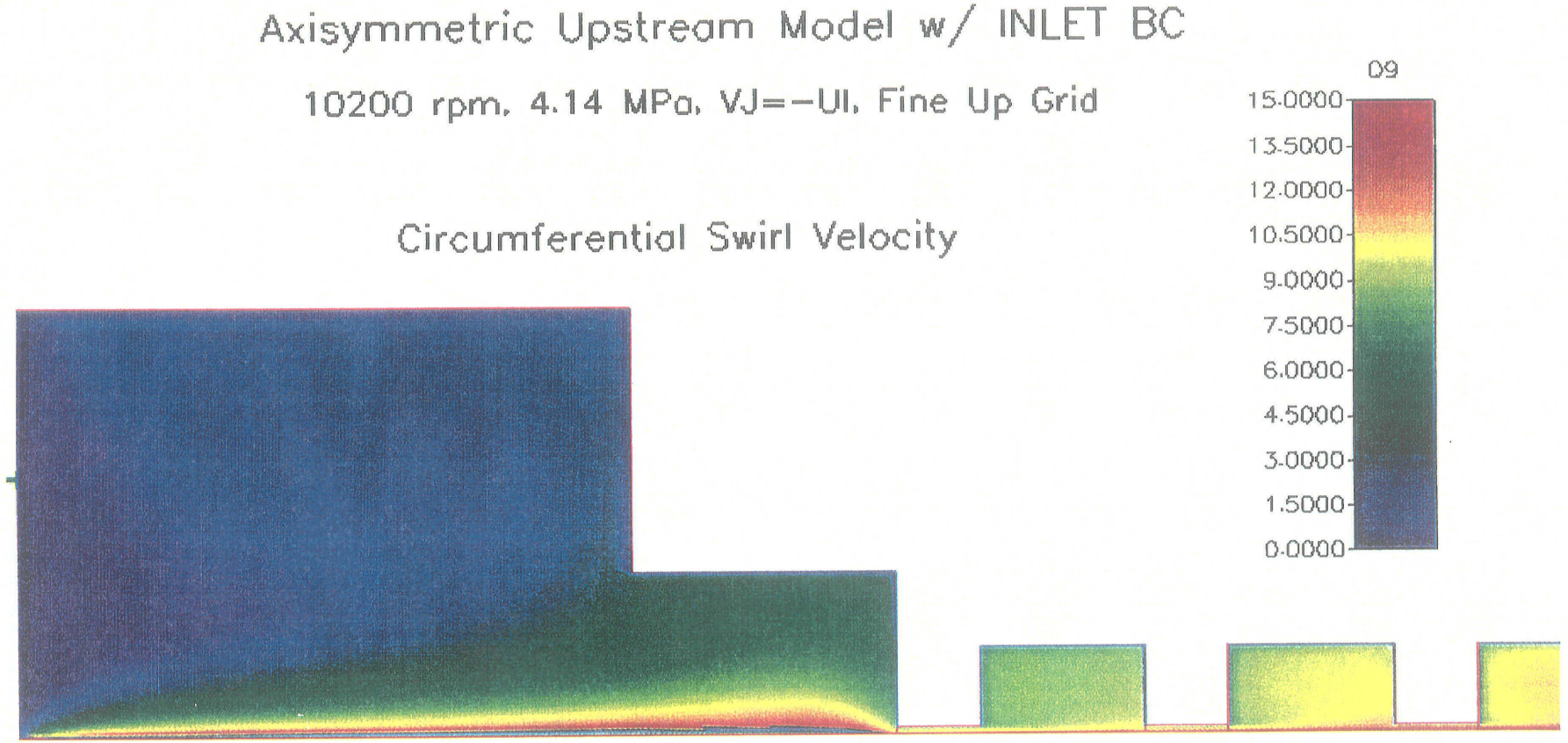

Figure 20 Development of Swirl Velocity, 10200 rpm (Normalized)

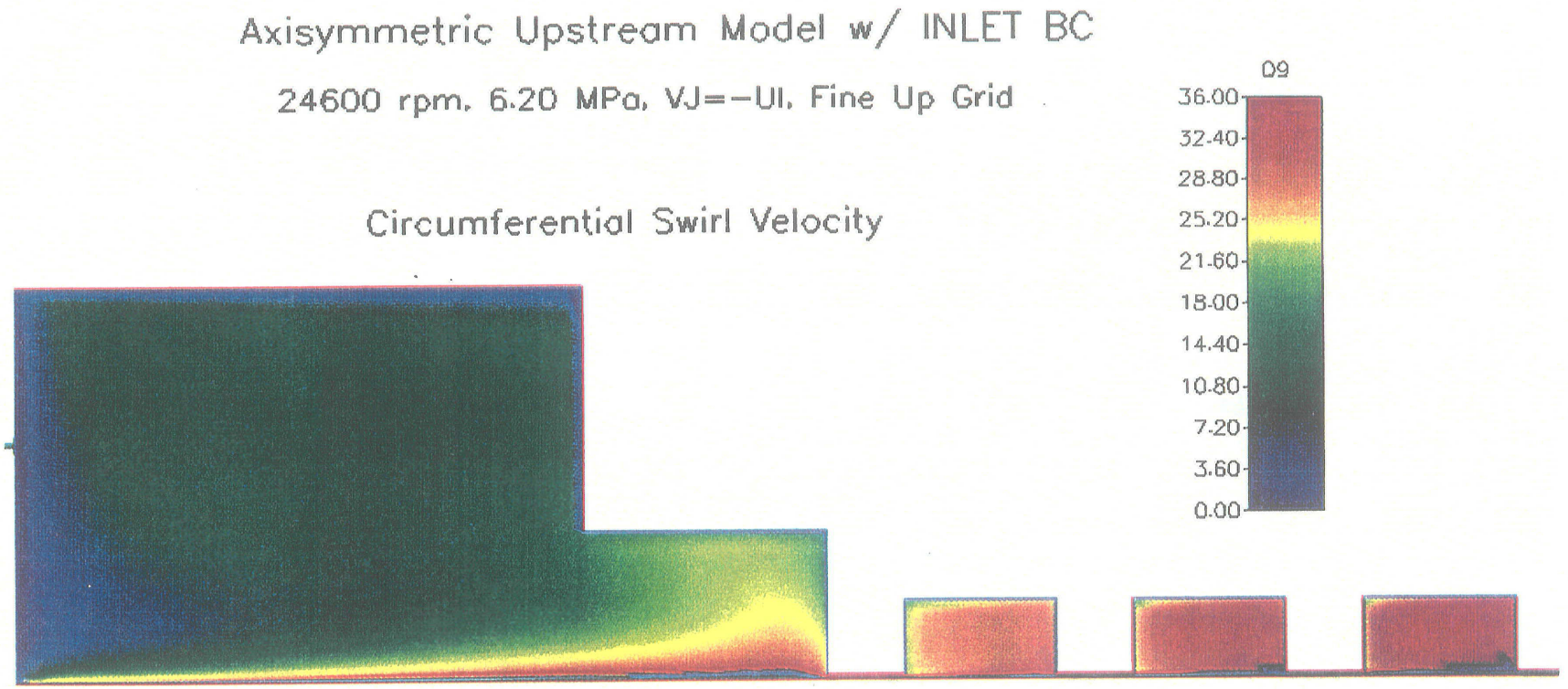

Figure 21 Development of Swirl Velocity, 24600 rpm (Normalized)

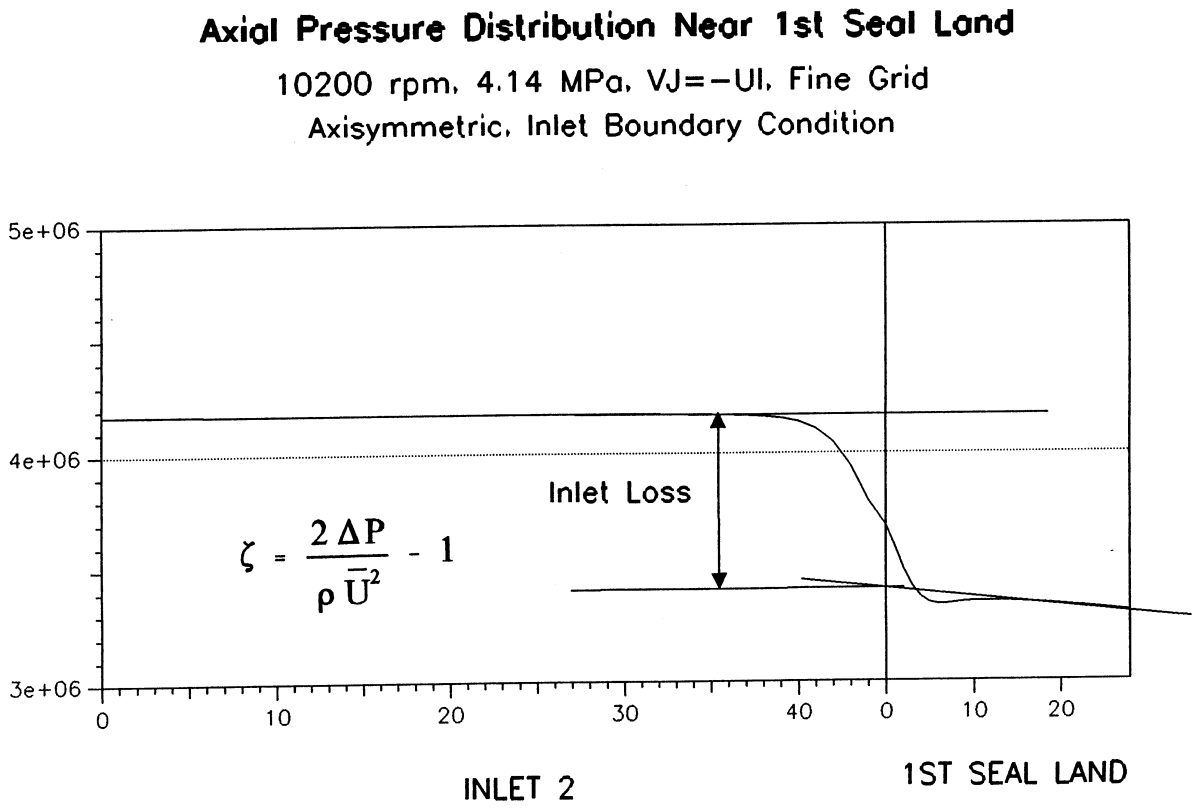

Figure 22 Inlet Loss of Pressure Entering 1st Seal Land

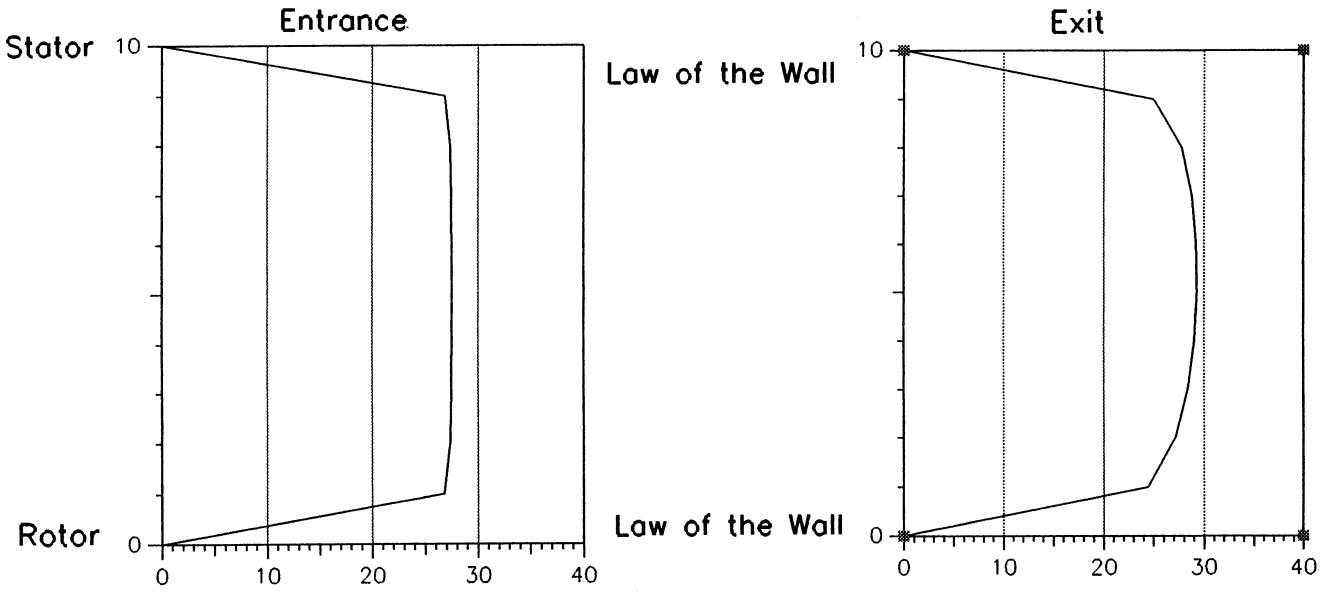

Figure 23 Development of Axial Velocity in 1st Seal Land
(Total-P BC at Seal Entrance)

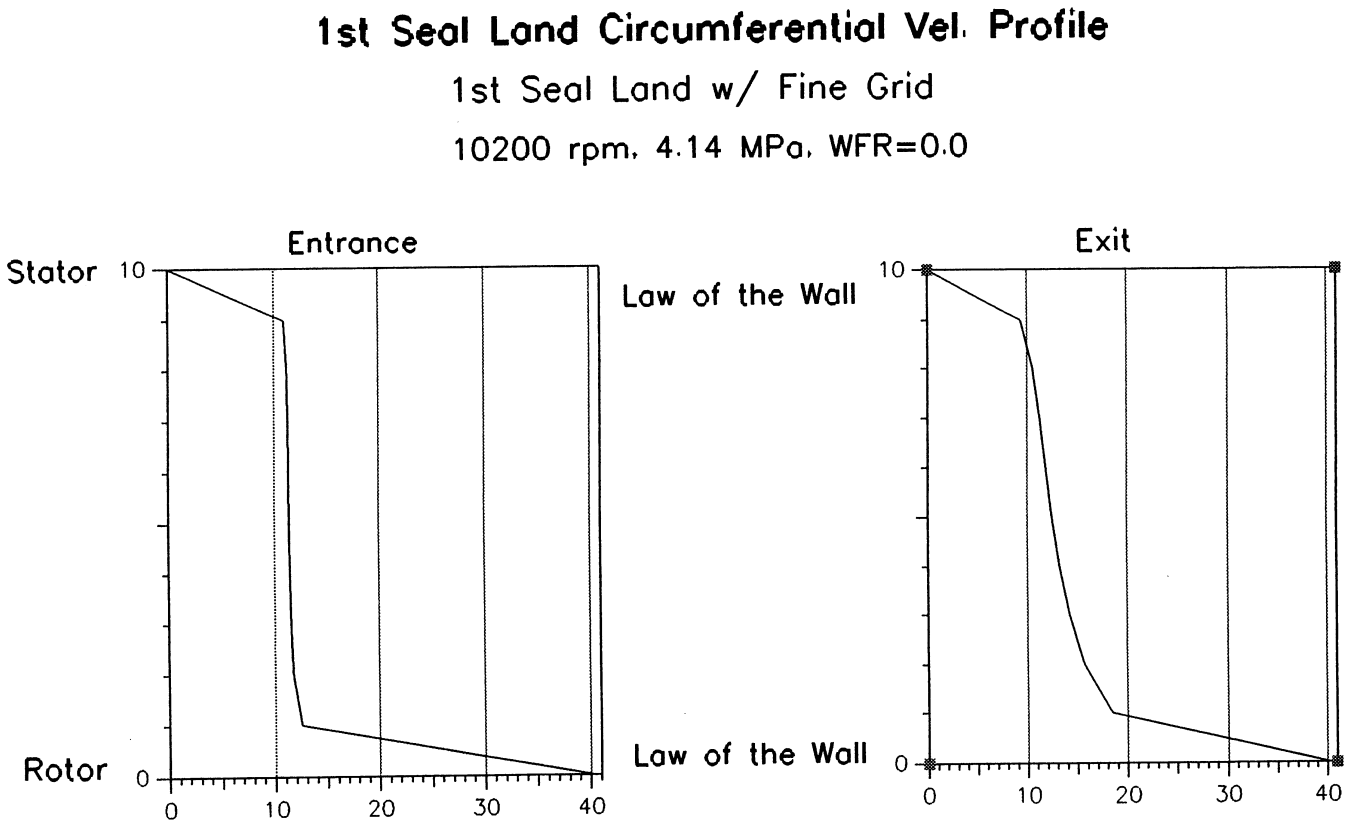

Figure 24 Development of Circumferential Velocity in 1st Seal Land (Total-P BC at Seal Entrance)

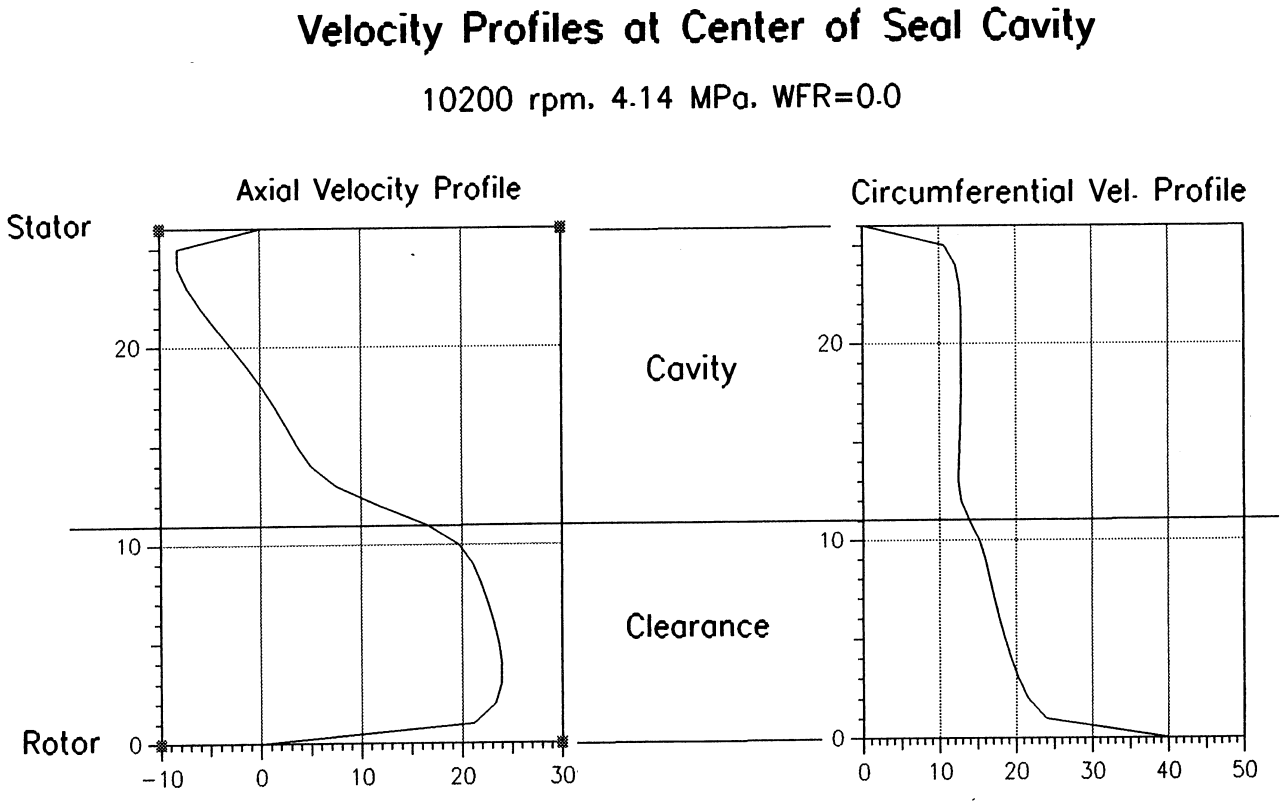

Figure 25 Velocity Distribution in Seal Cavity

Force Coefficients for Grooved Liquid Seal

10,200 rpm, Fine Grid-1, 4.14 MPa, Wrat=0.28, Ploss=0.63

	Computation	Experiment	3 Control Vol.
Kxx/Kyy (KN/m)	113	-5	-130
Kxy/-Kyx (KN/m)	307	740	99.8
Cxx/Cyy (KN-s/m)	3.11	4.81	4.59
Cxy/-Cyx (KN-s/m)	1.33	3.63	3.16
Mxx/Myy (kg)	1.34	5.19	3.59
Mxy/-Myx (kg)	0.34	-	-
WFR (Kxy / Cxx w)	0.09	0.14	0.02
Leakage (l/s)	0.70	0.82	0.82

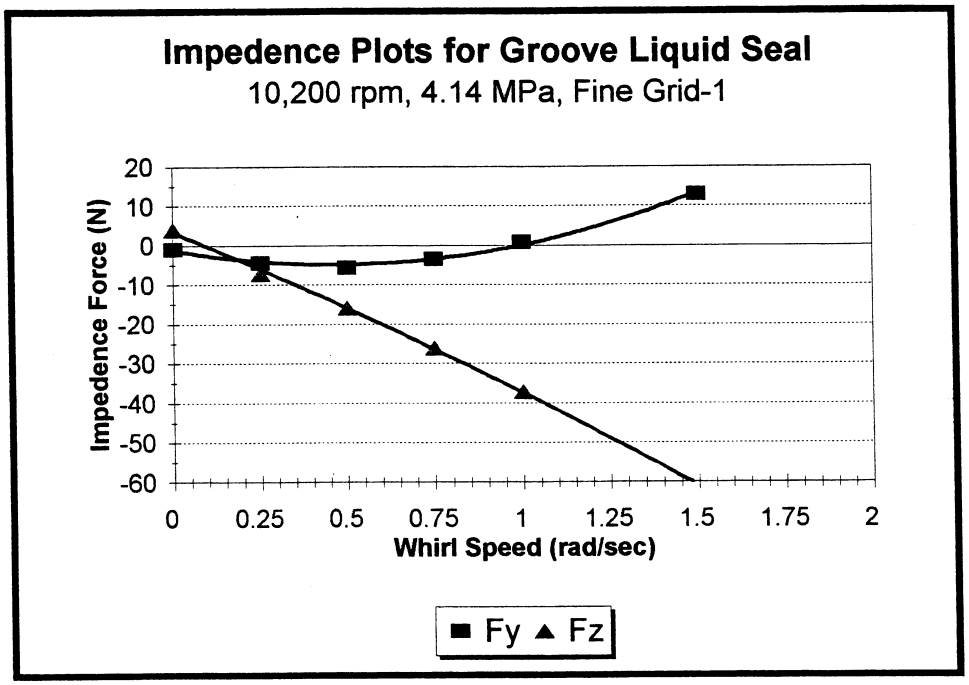

Table 6 Force Coefficients Using Boundary Conditions from Upstream Analysis (10200 rpm, 4.14 MPa, Wrat=0.28, Ploss=0.63)

Force Coefficients for Grooved Liquid Seal

24,600 rpm, Fine Grid-1, 6.20 MPa, Wrat=0.36, Ploss=0.70

	Computation	Experiment	3 Control Vol.
Kxx/Kyy (KN/m)	-880	-2490	-3560
Kxy/-Kyx (KN/m)	2028	3790	350
Cxx/Cyy (KN-s/m)	5.01	6.78	6.96
Cxy/-Cyx (KN-s/m)	2.99	8.84	7.21
Mxx/Myy (kg)	1.26	5.14	3.22
Mxy/-Myx (kg)	-0.06	-	-
WFR (Kxy / Cxx w)	0.16	0.22	0.02
Leakage (l/s)	0.81	0.97	0.897

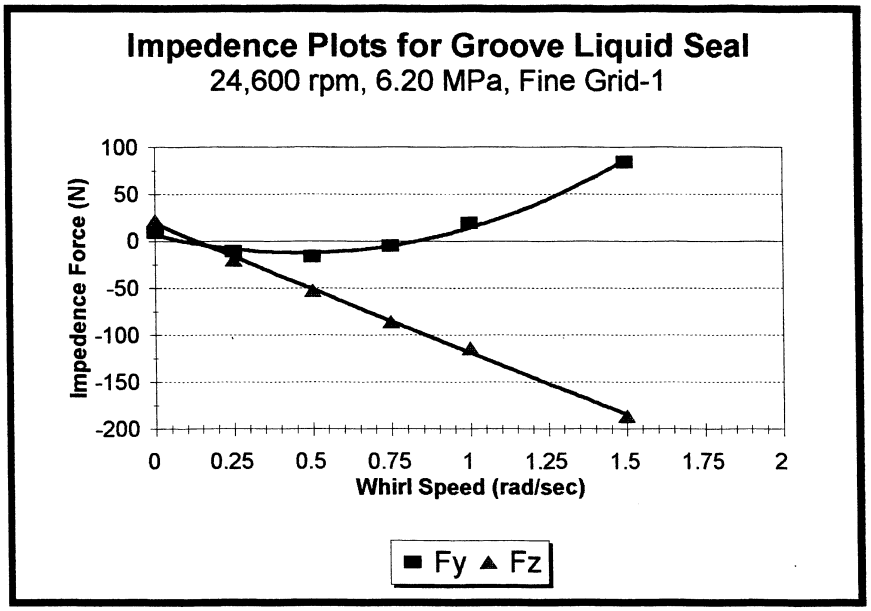

Table 7 Force Coefficients Using Boundary Conditions from Upstream Analysis (10200 rpm, 4.14 MPa, Wrat=0.28, Ploss=0.63)

SUMMARY

- Overall, CFD Calculations Provided Improved Predictions in Stiffness over Current Modeling Techniques (Worse for Damping and Inertia)
- Cross-Coupled Stiffness a Strong Function of Both Grid Density and Inlet Boundary Conditions
- Axisymmetric Upstream Analysis Provides Means to Obtain Seal Inlet Boundary Conditions
- CFD Used as a Final Analysis Tool, Bulk Flow and Control Volume Techniques Used as a Design Tool